UNIVERSITY OF TURKU

Developing and optimizing microfluidics platform for fabricating lignin nanoparticles

Master thesis
University of Turku
Department of Life Technologies
Molecular Systems Biology
Deependra Yadav

Supervisor:
Associate Prof. Hongbo Zhang
Pharmaceutical Sciences Laboratory
Faculty of Science and Engineering
Åbo Akademi University
Lab Supervisor:
Mr. Wali Inam
Pharmaceutical Sciences Laboratory

Master's thesis 2020

The originality of this thesis has been checked in accordance with the University of Turku Quality assurance system using the Turnitin Originality check service

Acknowledgement

I would like to express gratitude to the University of Turku for granting me scholarship to pursue my master's degree in Department of Life Technoogies, track Molecular Systems Biology. I would also like to thank to the coordinator of our department Dr. Paula Mulo for always being supportive and advising me throughout this journey and to assistant-prof Pauli Kallio for being my department supervisor.

I like to express my special thanks to my supervisor, associate-Prof Hongbo Zhang for giving me opportunity to participate with his research group and providing me an excellent environment for learning new technique and also encouraging me to work individually, that will be very fruitful for future.

I also like to express my special thanks to my lab supervisor Mr. Wali Inam, for teaching me all the technique used in this project and being so positive and encourage me when we are struggling to get result. I must have to thanks him for his suggestion in writing this thesis.

I appreciate the help of all the member of microfluidics lab for being so kind and helpful.

Finally, yet importantly I thank my parents for helping me through all the difficulties. I have experienced your guidance in everyday life and will keep on trusting you for my future. Thank you.

Abstract

Introduction: Lignin is a complex organic polymer, produced in large quantities as a by-product from pulp and paper industries. Despite of large-scale production, lignin is not being utilized for high value applications. Recently, researchers are showing greater interest in fabricating lignin-based nanoparticles for drug delivery and other application. However, it is challenging to fabricate lignin nanoparticles due to its complex chemical structure. Microfluidics technology used for nanoparticle synthesis because it works on microscale dimension with rapid and tunable mixing for better control over nanoprecipitation by controlling different parameters like flow rate, precursor and mixing time. The objective of this study is to develop method to fabricate lignin nanoparticles using microfluidics platform.

Material and methods: Two type of microfluidics chips were used for sequential precipitation, one consisting of two tapered ends and another with one tapered end. Kraft lignin (0.1%) was dissolved in ethylene glycol and lignin was precipitated with acetone and NaOH (0.1M). The fabricated nanoparticles were characterised by dynamic light scattering (DLS) and transmission electron microscope (TEM).

Result and Discussion: Two tapered end microfluidics chip were used to precipitate lignin because two solvent, acetone as counter solvent and NaOH as triggering precipitation was utilized, resulting nanoparticles of hydrodynamic particle size 162.5±1.82 nm, PDI 0.12±0.02 and zeta potential -24.6±2.17 mV at FRR 2:20:1 ml/hr (lignin:2ml/hr, acetone:20ml/hr, and NaOH:1ml/hr) were obtained. Whereas hybrid lignin nanoparticles (Ultra-small nanoparticles trapped in the lignin matrix) with hydrodynamic particle size of 129.73±5.91 nm, PDI 0.19±0.003 and zeta potential -15.5 mV were fabricated by sequentially precipitating kraft lignin with dual microfluidics chips setup (two tapered end and one tapered end chip). The solution from two tapered end chip was directly transferred at the rate of 23 ml/hr to the inner inlet of one tapered end chip, and precipitated at the FRR 3:20 ml/hr (3ml/hr:NaOH 0.1M) and 20ml/hr:acetone) as respective solution were infused in the outer most channel of one tapered end chip. Particles characterized with TEM showed hybrid nanoparticles consist of Ultra small primary particles were embedded in lignin matrix.

Conclusion: TEM image analysis suggest that we successfully developed method to fabricate hybrid lignin nanoparticles with the average size range from 20-50 nm utilizing microfluidics platform. Morphological analysis by TEM shows that nanoparticles are composed of ultra-small primary nanoparticles of 2-4 nm were trapped in matrix of different material. Further chemical characterization of this nanoparticles will help to understand its application. Keywords: lignin, nanoparticles, nanoprecipitation, microfluidics

Abbreviations

CNT	Carbon nanotube
CVP	Chemical Vapor Deposition
DLS	Dynamic Light Scattering
FLS	Shear Lift Force
FRR	Flow Rate Ratio
HFF	Hydrodynamic Flow Focusing
LNP	Lignin Nanoparticles
PDMS	Polydimethylsiloxane
PDI	Polydispersity Index
PZC	Point of Zero Charge
Re	Reynolds number
SDR	Spinning disc reactor
TEM	Transmission Electron Microscope
WLF	Wall lift force

Contents

1. Introduction

1.1 Microfluidics

Microfluidics is the science of studying the behaviour, control, and manipulation of fluids geometrically controlled to sub-millimeter dimensions, involving the integration of fluids with micro and nanostructures devices (M. Zhang et al., 2009). Microfluidics is an interdisciplinary subject, applicable to the wide range of fields such as microtechnology, engineering, biotechnology, chemistry, physics, and materials science. The development of micro-miniaturized analytical device extends the application of microfluidics to biomedical analysis, chemical sensing, genetic analysis and metabolic monitoring (Van Den Berg & Andersson, 2004).

Microfluidics is widely applicable for the fabrication of micro and nanoparticles because of the possibility to manipulate the flow rate. Microfluidics provides an alternative approach to the conventional methods of preparing nanoparticles. In comparison to the conventional method, microfluidics device requires small reagents, short response time, low cost and reduce cross-contamination (Igata et al., 2002). Microfluidics devices consist of fluidic channels with a minimum of one dimension in millimeter scale. Such fluidics channel allows high surface to volume ratio and requires small volumes of reagents. The high surface to volume ratio allows a high rate of heat and mass transfer that can be used for heat exchange modules for high power electron (Paik et al., 2008). The feature of the microfluidic device is represented in figure 1.1.

The history of microfluidics devices dates to 1950, when the biological molecules of fluids were controlled in the range of nano and sub-nanoliter range were made for the basics of inkjet technology. Later, in 1979 the development of a silicon-miniatured gas chromatography at Stanford University is considered as the first microfluidics device (Terry et al.,1979). Nowadays, microfluidics is a demanding technology to fulfill the growing needs of health care due to less sample processing time with reliable and accurate result. It can operate small quantities of fluid within defined dimensions onto microfluidic devices for on-chip testing (Minteer, 2006). The fluids volume required for

the microfluidics are measured in microliters (10^{-6} l) to picolitres (10^{-12} l) and flow rates are in the range of few microliters per minute (Stone et al., 2004). The flow within the microfluidic devices is laminar which allow mixing by molecular diffusion.

In bulk synthesis mixing accomplishes in longer duration. Whereas small distances in microfluidics channel allow complete mixing within few seconds or minutes (Janasek et al., 2006).

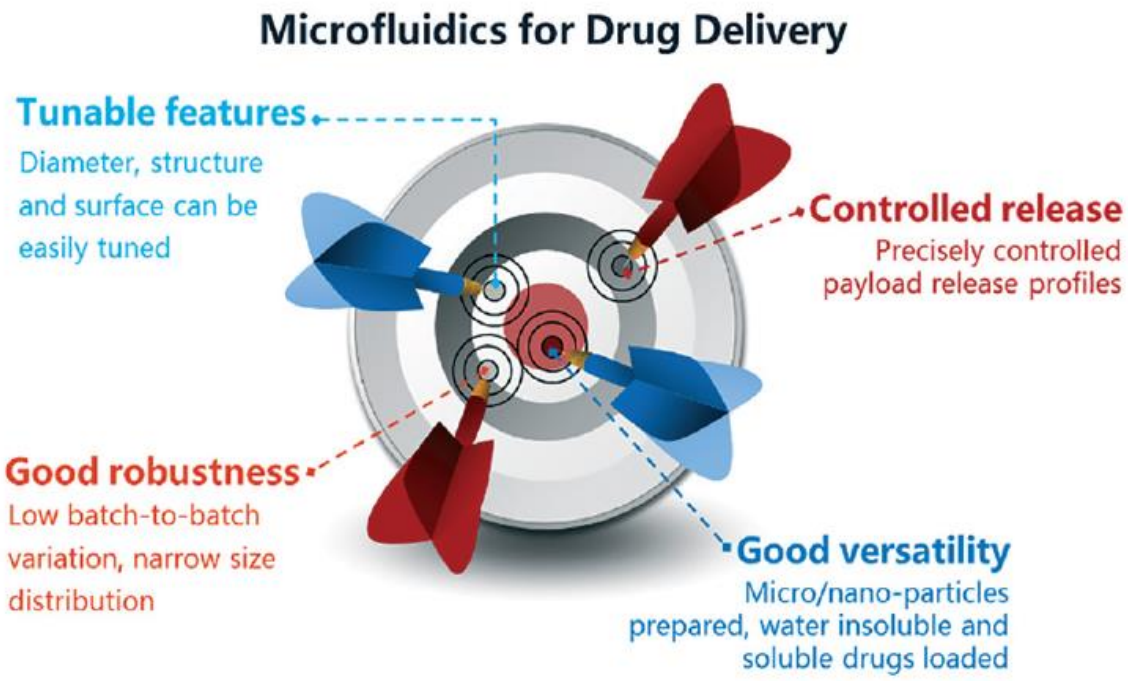

Figure 1.1 Schematic representation of microfluidics device advantage toward the fabrication of nanoparticles. Reprinted with permission from reference (Liu et al., 2017).

1.1.1 Materials for microfluidics devices

Physical characteristics such as flexibility, electrical conductivity, nonspecific adsorption, optical transparency, cellular and solvent compatibilities are important parameters for choosing a material for microfluidics devices (Nge, Rogers, & Woolley, 2013). Microfluidics devices can be manufacture from different materials, the early devices were made of inorganic materials like glass and silicon via photolithography. The glass is still popular for device fabrication. Due to rapid prototyping, polymers chip including polydimethylsiloxane (PDMS) is commonly used in the research lab (Pallandre et al., 2006). Cellulose-based materials like paper are also being used for the

fabrication of microfluidic devices (X. Li et al., 2012). Glass capillaries are a better choice for fabricating the microfluidics devices due to its better tolerant to wider range of solvents, flexibility regarding application in drugs encapsulation and it also resistance to high pressure and flow rates. Glass microfluidics device is manufactured by pulling capillaries into a fine tip with the precise orifice, placed co-axially within a large capillary and glued those capillaries onto a glass slide (Liu et al., 2017).

1.1.2 Mechanism of microfluidics

There are several methods for the pumping of solution through microfluidics channels, but the most common methods are hydrodynamic and electroosmotic flow-based pumping. The hydrodynamic pumping includes the application of pressure, via a syringe pump or hydrostatic and centrifugal forces whereas, electroosmotic flow includes voltage difference in microchannel that features charged surface (Burger & Ducrée, 2012).

The behaviour of the fluid flow can be explained by the Reynolds number. The Reynolds number is a dimensionless parameter and describe the ratio of inertial forces to viscous force of liquid in motion (Malhotra & Ali, 2018). Equation can be represented as,

$$Re = \frac{Inertial\ Force}{Viscous\ Force} = \frac{\rho u L}{\mu}$$

Where, u is the average flow velocity, L is the characteristic length, μ is dynamic velocity and ρ is the density of the fluids. With increasing viscous force Re decreased resulting in laminar fluid flow. While with increasing inertial force, Re increased resulting in turbulent flow. Quantitatively, fluid flow with higher Reynolds number approximately 2300 consider as transition from laminar to turbulent flow (Liu et al., 2017).

Inertial microfluidics work on inertial migration phenomenon where particles dispersed randomly to different equilibrium positions. The inertial migration is controlled by two inertial forces: a) the shear gradient lift force (FLS) and b) the wall lift force (WLF). FLS pushes the particle away from the channel centre due to curvature of fluid velocity

and interaction with particles. While WLF counter interaction between particle and wall of channel, resulting repulsion of particles away from the wall. These two inertial lift forces keep particles in the equilibrium position. Whereas, fluid near the centreline of channel have higher momentum compare to fluid near wall of channel which causes stagnant fluid near the wall of channel, resulting two counter-rotating movements of fluids called Dean vortex. This secondary flow produced another drag force perpendicular to flow of fluid. Both inertial lift force and secondary flow play important role in acquiring size-based particle separation (J. Zhang et al., 2016).

1.2 Nanotechnology and nanoparticles

Nanotechnology can be defined as "the intentional design, characterization, production, and application of materials structures, devices and systems by controlling their size and shape in the nanoscale range (1 to 100 nm)" (B. Y. S. Kim, Rutka, & Chan, 2010). Nanoparticles or nanomaterials can be commonly defined as a particle having diameter of the range of 1 to 100 nm. There is no internationally accepted standard definition of nanoparticles, the different organizations have their own opinion in defining nanoparticles. According to US Food and Drugs Administration (USFDA) nanoparticles define as "materials that have at least one dimension in the range of approximately 1 to 100 nm and show dimension dependent phenomena". Nanoparticles have a high ratio of surface area to volume with tunable properties which is very useful for targeting site specific drug-delivery (Xia et al.,2009).

In recent year, researchers are interested to manufacture hybrid nanoparticles, hybrid nanoparticles consist of at least two different materials. Such hybrid nanoparticles have improved properties to achieve multiple function that cannot be possible with single particles. There are several hybrid nanoparticles are reported like core-shell, yolk-hell, heterodimer, dot-in-nanotube, nano-branch, Janus nanoparticles etc (Mohapatra et al., 2018). Microfluidics nanoprecipitation is also used to produce hybrid nanoparticle by encapsulation of inorganic nanoparticles such as porous silicon, iron oxide, gold and quantum dot nanoparticle within the organic nanomatrix (Liu et al., 2017).

Nanoparticles can be categorized into four types based on their material of synthesis: (1) Carbon-based nanoparticles, these particles mostly contain carbon and morphologies are

hollow tubes, ellipsoids or spheres. Examples are carbon nanotubes (CNT), graphene nanosheets and nanodiamond; (2) Inorganic-based nanoparticles, include metal and metal oxide nanoparticles. Such nanoparticles can be synthesized into metal like Au, Ag and Cu and metal oxide such as ZnO, TiO_2, Fe_2O_3; (3) Organic-based nanoparticles mostly contains organic matter such as nanostarch, nanocellulose, liposomes and polymers; (4) Composite-based nanoparticles are those nanoparticles that integrate nanoparticles with other nanoparticles or nanoparticles that merged with bulk-type materials such as hybrid nanofibers, or more complicated structure like metal-organic framework and mixed metal oxide (Janczak & Aspinwall, 2012; Samyn et al., 2018).

Nanoparticles fabrication is generally categorized into bottom-up and top-down methods. Top-down approach is the process of destruction where bulk material is broken down into nanometric scale particles (nanoparticles). The most commonly used method for top-down approach are mechanical milling, sputtering, laser ablation and thermal decomposition. Bottom-up approach is a process in which nanoparticles are built up from atomic level to nano-levels. The most common bottom-up methods are Sol-gel, spinning, chemical vapor deposition (CVD) and pyrolysis (Ganesh Kumar et al., 2017).

1.2.1 Sol-gel

Sol-gel method is the most preferred method of bottom-up approach, sol refers to colloidal suspension of solid nanoparticles in a liquid phage and gel is 3D interconnecting network formed within the phases. Sol-gel methods took place in two step reactions, at the first step solid nanoparticles are dispersed in solution to produce Sol. Then polymerization took place to form an interconnecting network between phases (gel). Finally, hydrolysis took place to extend polymer nanoparticles 3D network inside the liquid. Here polymer act like a nucleating agent to boost the growth of layered crystal. Due to layered crystal growth, the polymer seeps between layers to form nanoparticles (Alexandre & Dubois, 2000).

1.2.2 Spinning

Spinning is bottom-up approach that uses spinning disc reactor (SDR) for the fabrication of nanoparticles. It consists a rotating disc inside the reactor. The reactor is filed with the nitrogen or other types of inert gases that help to get rid of oxygen and avoid chemical reaction. The physical parameters like temperature is controlled inside the reactor (Tai et al., 2007). The disc can be rotated at several speed that causes atoms to fuse together and precipitate. Finally, particles can be collected and dried. The characteristics of synthesised nanoparticle can be determined by various operating parameters in SDR such as disc rotating speed, liquid flow rate, liquid/precursor ratio, disc surface etc (Mohammadi, Harvey, & Boodhoo, 2014).

1.2.3 Chemical vapour deposition (CVD)

Chemical vapour deposition (CVD) is a process of depositing solid material (thin film or powder) from vapour by chemical reaction that occurs on or in the vicinity of heated substrate surface. The experimental condition such as substrate temperature, substrate material, composition of reaction gas mixture can be varied to obtain varieties of particles. CVD process produces highly pure, uniform nanoparticles while its gaseous by-products are highly toxic (Bhaviripudi et al., 2007; Ealias & Saravanakumar, 2017).

1.2.4 Pyrolysis

Pyrolysis is a common method used for the large scales production of nanoparticle. The precursor (liquid or gas) is fed into the furnace through an orifice at high pressure to burned (Kammler, Mädler, & Pratsinis, 2001). The resulting by-product gases are classified to retrieved nanoparticles. Nowadays, laser and plasma are used instead of flame in some of the furnaces to produce high temperature for easy evaporation (Ealias & Saravanakumar, 2017).

1.3 Advantage of microfluidics for nanoparticles synthesis

Nanoparticles can be used for different application such as drug delivery, photovoltaic cells, energy generation, gene therapy and biochemical sensing. For the effectiveness of application, nanoparticles must be exhibit in a uniform size and shape with identical physiochemical properties (Boken et al., 2016). In microfluidics systems chemical reaction is carried out on a microscale including temperature control, fast mixing by diffusion. However, in conventional batch process mixing is slow with low effective control on mixing and temperature. The optimization of circumstances for nanoparticles fabrication in conventional methods is difficult. The production of nanoparticle by conventional methods takes minutes or hours. Hence, it is not possible to derive intermediate solution with shorter lifetime compare to production time. The intermediate solution decomposed during accumulation in conventional method whereas unstable intermediate solution can transfer to another location and can be used in following reaction before it can decompose in microfluidic methods (Boken et al., 2016; Park et al., 2010). Microfluidics provide continuous-flow methods for preparing micro- and nanoparticles in single phage or multiphase solution. (Boken et al., 2016; Tsaoulidis & Angeli, 2015). There are different advantage of using microfluidics device for the fabrication of nanoparticles such as processing accuracy, efficiency , cost efficiency from low consumption of source material and reagents, rapid result production for fine tuning properties of synthesized particles, multi-step platform design flexibility and eco-friendly process as it uses non-toxic chemicals and reagents (Boken et al., 2016; Yeo et al., 2011).

1.4 Mechanism of microfluidics precipitation

Mechanism of nanoprecipitation and nanoparticle synthesis can be explained in three steps: (a) nucleation, (b) growth and (c) nanoparticle formation. Thermodynamic and kinetic studies suggested that at first several insoluble polymer molecules rearrange or

fused together during solvent change and form a nucleus, such process is called nucleation. The second stage is growth, in which particle size increases with fusion of nascent particles with the help of electrostatic force. The growth stage last until the brush borders are forms on the surface of nanoparticles. Finally, in third stage particles deposit with low insertion barrier, but it slightly changes the size of particles (Johnson & Prud'homme, 2003). The growth stage of nanoprecipitation follows two mechanism, first is the diffusion limit growth process where solute molecules stick onto the nuclei surface until the solute equilibrium concentration is achieved. Second is diffusion limited cluster-cluster aggregation where collision of random nuclei to form dense structures when the nuclei concentration is high (figure 1.2) (Lepeltier et al., 2014).

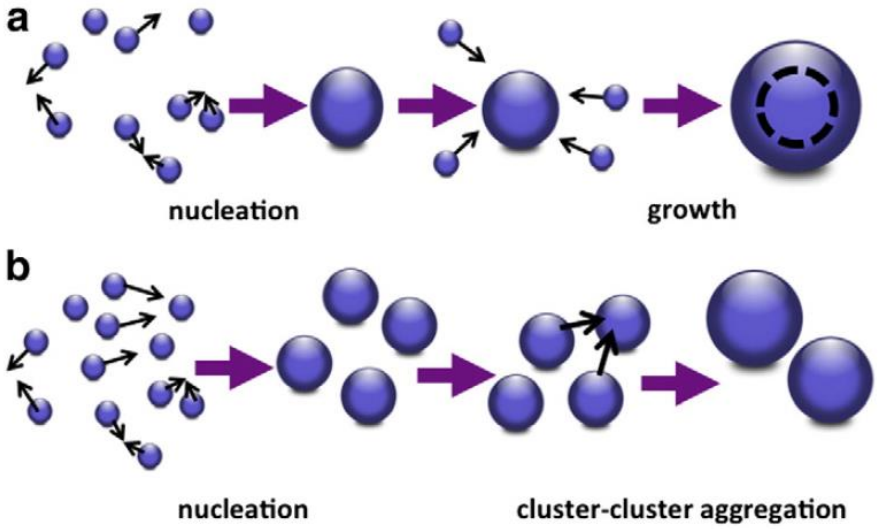

Figure 1.2 Schematic representation of (a) nucleation and diffusion limited growth process (b) diffusion limited cluster-cluster aggregation. Reprinted with permission from the reference (Lepeltier et al., 2014).

Microfluidics devices for nanoparticle synthesis can be categorized into two group based on hydrodynamic flow focusing (HFF) technique: (a) two-dimensional (2D) and three-dimensional (3D) HFF. 2D-HFF consists of three inlets, the inner stream with lower flow rate is compressed and fussed by two sheath flow from two sides in the horizontal plan (figure 1.3). As the result of compression the mixing time will be significantly reduced due to decrease in the diffusion length (M. Lu et al., 2016). 3D-HFF is also called coaxial microfluidics device, where the central stream is squeeze both horizontal and vertical direction to achieve an ideal focusing. However, the fabrication of 3D-HFF is more complicated than 2D-HFF. 3D-HFF consists of two different size concentric

capillaries, one with smaller diameter and another with larger diameter capillary coaxially aligned in each other by hand (Liu et al., 2017).

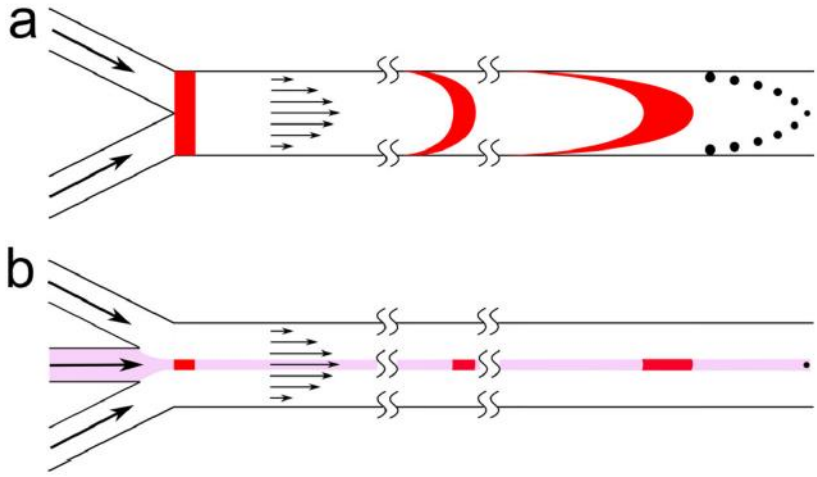

Figure 1.3 Schematic representation of 2D-HFF device. (a) device without an additional inlet for the nanoparticle stream, fluid near the edge spends the longer time. (b) HFF keep the reaction to the centre of the channel, providing more uniform reaction time and synthesized product distribution. Reprinted with permission from reference (Liu et al., 2017).

Based on flow behaviour, microfluidics utilized two general principle for the fabrication of nanoparticles a) continuous flow and b) segmented flow with liquid-liquid or gas-liquid interaction.

1.4.1 Continuous flow

Continuous flow system is the simple and commonly used microfluidic technique for nanoparticle fabrication. In single-phage continuous system (figure 1.3), precursor fluids flow continuously through the microchannel where nucleation and growth phage took place (M. Lu et al., 2016). The flow rates, concentrations of reagent, time and reaction temperature can easily be control in this system. Moreover, nanoparticles can be easily manipulated and modify by adding required reagents at any time throughout the process (Uson et al., 2018). The output of the single-phase continues methods can be improved by adjoining several similar microchannels parallelly on the same lamina (Dunne et al.,

2015). HFF technique is a type of continues flow microfluidics, in which a sheath solution with higher flow rate is applied to compress a central solution with a lower flow rate from all the direction. Therefore, the diffusion distance and mixing time is reduced and the quality of synthesized nanoparticles is improved. The size of the nanoparticles can be controlled by changing the flow rate of central and sheath solution. Moreover, due to the reaction is restricted within a focused central flow and the channel wall is isolated from the precursors to avoid clogging, hence the continues formation of nanoparticles for a long period can achieved (X. Zhao et al., 2020).

1.4.2 Segmented flow

Segmented flow microfluidic systems require microfluidic devices of various geometrical designs such as T-junction, co-flow and flow-focusing to generate segmented flow between liquid-liquid and liquid-gas interaction. In the liquid-liquid segmented flow, the droplet is produced due to the instability of dispersed phage such as water-in-oil or oil-in-water emulsions. The parameter that can affect the droplet formation are microfluidic chip construction, solution viscosity and flow rate, which affect the resultant size and structure of nanoparticles (W. Li et al., 2018; X. Zhao et al., 2020). In a gas-liquid segmented flow, gas bubbles are pumped into microfluidics chip in a controlled manner and it dispersed in continuous liquid phase. Nanoparticles synthesized by gas-liquid segmentation are of high quality and synthesized continuously because of it efficient mixing capacity, rapid heat and mass transfer provided by each microdroplet (X. Zhao et al., 2020).

1.5 Lignin and its chemical structure

Lignin can be defined as a complex mixture of organic polymers with high molecular weight (Tribot et al., 2019). The general nature of isolated lignin is amorphous brown colored and one of the significant properties of lignin is that it absorbs UV-light. The first time lignin was isolated in 1956 using dioxane-water (96:4 ratio) from the spruce wood called milled wood lignin (de Gonzalo et al., 2016). Lignin is a phenylpropanoid biopolymer, found in the plant cell wall. The plant biomass is made of cellulose, hemicellulose and lignin. Lignin present in between cellulose and hemicellulose. Lignin

is generally present in vascular plant tissue, where it provides mechanical support, physical strength and rigidity to the cell structure. Plant biomass mainly consists cellulose (38–50%), hemicellulose (23–32%) and lignin (12–25%) component (de Gonzalo et al., 2016; Sun & Cheng, 2002).

In 1977, Adler presented the first structure of lignin where he describes lignin as "highly branched biopolymer containing various methoxy, carboxylic, phenolic and aliphatic hydroxyl, and carbonyl functional groups" (Adler, 1977). Lignin composition varies from species to species. Mostly lignin is composed of carbon, hydrogen, oxygen and ash. Its chemical formula is $(C_{12}H_{34}O_{11})_n$ (Hu & Hsieh, 2016) and molecular weight in average between 1000 to 20000 g mol^{-1} depending upon methods used for extraction (Norgren & Edlund, 2014). Lignin structure composed of three phenylpropane monomer or monolignol units (Figure 1.4) of p-coumaryl (p-hydroxyphenyl (H) units), coniferyl (guaiacyl (G) units) and sinapyl alcohol (syringyl (S) units) (Kun & Pukánszky, 2017). The amount of lignin present depends on the type of plant biomass (Itoh et al., 2003; Suhara et al., 2012). Mainly, the higher amount of lignin is present in three types of biomass such as softwood content 25-35 % of lignin which contain G units, hardwood content 18-25 % of lignin where G and S units are present (Silverstein, Chen, Sharma-Shivappa, Boyette, & Osborne, 2007; Valášková et al., 2007) whereas grasses contain lowest percentage of lignin (10-19 %) contains all the three phenylpropane (G, S and H) units (Hendriks & Zeeman, 2009).

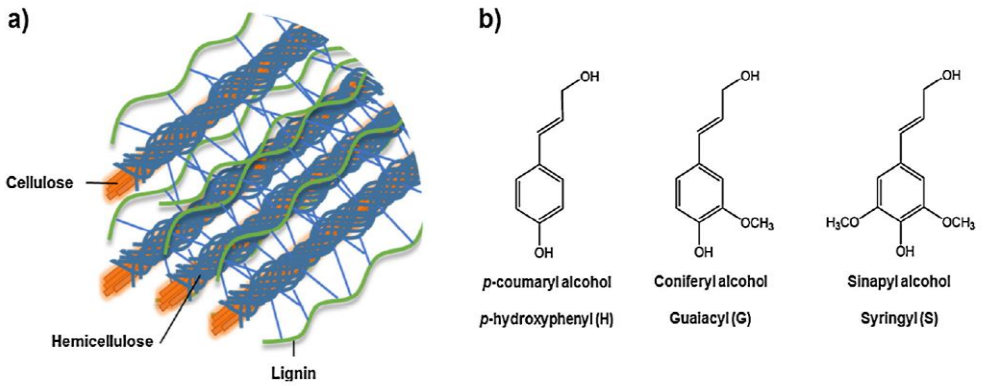

Figure 1.4 a) Representation of lignin position in cell wall and b) Chemical structure of lignin monomer units. Reprinted with the permission from reference (Figueiredo et al., 2018).

The guaiacyl unit (G) have one OCH_3 group obtain from coniferyl alcohol, syringyl units (S) consists of two OCH_3 group acquire from sinapyl alcohol and p-hydroxyphenyl units (H) derived from p-coumaryl alcohol have no OCH_3 groups. Lignin monomers are covalently interconnected during biosynthesis to form a polymer with primary linkage of C-C (condensed bonds) and C-O-C (ether bonds) (Henriksson, 2017). Lignin molecules consist of different linkage, β-O-4, 5-5, β-5, 4-O-5, β-1, dibenzodioxocin and β- β linakge. Among the linkage more than 50% is β-O-4 ether linkages present in lignin molecules (figure 1.5)(Laurichesse & Avérous, 2014).

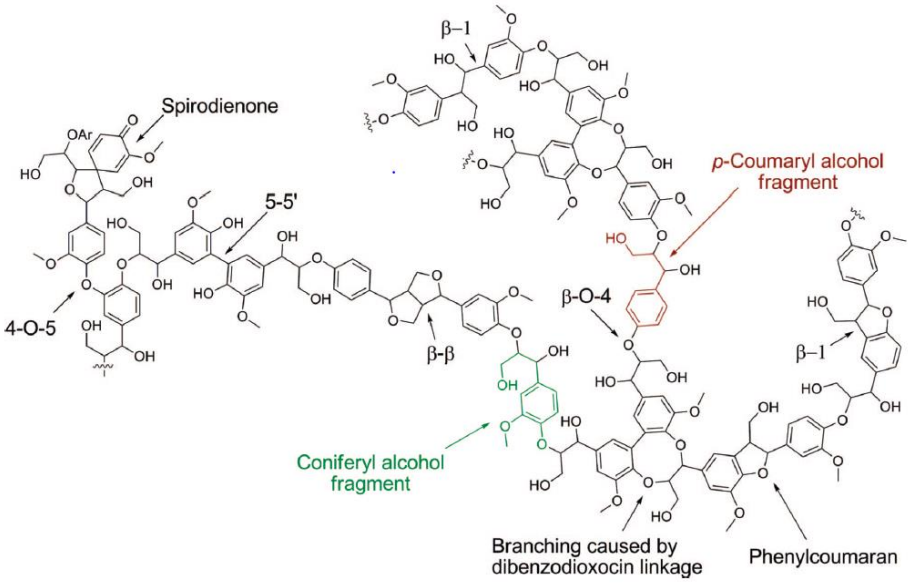

Figure 1.5 Schematic representation of softwood lignin chemical structure. Reprinted with the permission from reference (Zakzeski et al., 2010).

The composition of softwood and hardwood lignin is different in the presence of the p-coumaryl, coniferyl, and sinapyl alcohols. Softwood lignin consists of approximately 90% of coniferyl alcohols, whereas hardwood lignin consists of approximately uniform quantities of coniferyl alcohol and sinapyl alcohol. The structure of hardwood lignin is comparatively linear than softwood lignin because of methoxy group present on the aromatic ring that block the initiation of 5-5 or dibenzodioxocin linkage (Zakzeski et al., 2010).

1.5.1 Type of lignin

Based on the different extraction process lignin can be categorized as kraft lignin, lignosulphonates lignin, soda lignin and organosolv lignin. Commercially available extraction process of lignin is mainly classified into sulphur and sulphur-free process, sulphur process includes kraft and lignosulphonates lignin whereas sulphur-free process includes soda and organosolv lignin (Laurichesse & Avérous, 2014). Each of the lignin types has their particular chemical structure and properties. Generally, lignin is resistant to decaying, UV absorbance, high stiffness and antioxidants are the unique properties of the lignin. Hence, lignin can be utilized to synthesis valuable products (Beisl et al., 2017).

1.5.1.1 Soda lignin

Soda lignin obtain by soda pulping process, such cooking process mainly uses annual crops like flax, straws, bagasse and some hardwoods (Rodríguezv et al., 2010). Soda lignin is utilized to produce phenolic resin, animal nutrition and dispersants. Soda lignin is also suitable for the synthesis of polymer (Vishtal & Kraslawski, 2011).

1.5.1.2 Organosolv lignin

Organosolv lignin is a comparatively pure form of lignin with low molecular weight. It is highly soluble in organic solvent and partially soluble in water. Due to its lower molecular weight, it can be used as adhesives and binder. It also uses as filler in the formulation of inks, varnishes and paints (Belgacem et al., 2003; Lora & Glasser, 2002).

1.5.1.3 Lignosulphonates lignin

Lignosulphonates lignin is water soluble and of higher molecular weight. It consists of different functional groups such as phenolic hydroxyl groups, carboxylic groups and sulphur containing groups. Lignosulphonates lignin is used for the fabrication of detergents, glues, animal feed, surfactants, adhesives and cement additives (Laurichesse & Avérous, 2014; Vishtal & Kraslawski, 2011).

1.5.1.4 Kraft lignin

Kraft lignin is fabricated by sulphate (kraft) cooking process, which contain approximately 85 % of the total lignin production in the world (Tejado et al., 2007). In kraft cooking process, about 90-95 % of the lignin is dissolved in the cooking liquor solution containing sodium hydroxide and sodium sulfide. Around 630,00 tons of kraft lignin is produced annually. However, lignin is mostly utilized for the low value application such as the production of heat and energy (Chen, 2015). Around 100,000 tons of lignin is used for the other product and applications such as carrier for fertilizer and pesticides, carbon fibers, blends with thermoplastic polymers, ion-exchange resin, vanillin, hydroxylated aromatics, aldehydes and aliphatic (Holladay, Bozell, White, & Johnson, 2007; Vishtal & Kraslawski, 2011).

Table 1. Chemical compositions of kraft, soda, organosolv and lignosulphonate lignin. Reprinted with the permission of reference (Gao & Fatehi, 2019a).

Parameter	**KL**	**SD**	**OL**	**LS**
Ash(mass%)	0.5-3.0	0.7-2.3	1.7	4.0-9.3
Moisture content (mass%)	3.0-6.0	2.5-5.0	7.5	5.8
Carbohydrates (mass%)	1.0-2.3	1.5-3.0	1-3	…
Acid insoluble lignin (mass%)	91.3	86.4	92.3	…
Acid soluble lignin (mass%)	1-5	1.0-11.5	<2	…
Solvent	Alkali, organic	Alkali	Organic	Water
Nitrogen (%)	0.05	0.2-1.0	0-0.3	0.02
Sulphur (%)	1.0-3.0	0	0	3.5-8.0
OCH_3 (%)	10.47	19.3	15.2	8.7
Phenolic hydroxyl groups (%)	4.1	4.5	3.3	2.2
Aliphatic hydroxyl groups (%)	10.09	3.1	3.5	…
Carboxylic group (%)	7.1	6.9	2.86	4.3
Sulphonate groups (%)	…	…	…	12.23
Carbonyl groups (%)	2.91	2.13	3.94	4.50
Free C-3 and C-5 per C9 formulae	0.4	0.36	0.21	0.24
Molecular weight (g/mol)	1500-5000	1000-3000	500-5000	1000-50000
Polydispersity	2.5-3.5	2.5-3.5	1.5-2.5	4.2-8

Abbreviations: - KL: Kraft lignin, SD: Soda lignin, OL: Organosolv lignin, LS: Lignosulphonate lignin

1.5.2 Chemical modification of lignin

The phenolic and aliphatic hydroxyl groups of lignin can be easily modified to produce new material. Lignin can be utilized with or without chemical modification, based on their application. Chemically unmodified lignin can be used as antioxidant, UV-light stabilizer, flame retardant and additive to promote plasticity. Chemically modified lignin can be used in polymer synthesis, fuels and chemicals (Laurichesse & Avérous, 2014; Pouteau et al., 2003). The chemical modification of lignin can be done by four methods: (a) lignin depolymerization; (b) synthesis of new chemically active sites; (c) functionalization of hydroxyl groups and (d) production of lignin graft copolymers (Ragauskas et al., 2014).

1.5.2.1 Lignin depolymeraization

Lignin depolymerization or fragmentation is a process where lignin raw material is converted to valuable products. Lignin is a suitable raw material for synthesizing low molecular mass compounds such as aldehydes, aliphatic acids and vanillin (Lin et al., 2011). Lignin fragmentation help to understand the chemical composition and structure of lignin to produce useful material from lignin raw material. Several methods such as pyrolysis, oxidation, hydrogenolysis, hydrolysis and gasification are used for lignin depolymerization (Pandey & Kim, 2011).

1.5.2.2 Synthesis of new chemical active sites

Lignin chemical structure has various functional groups such as hydroxyls, methoxyls, carbonyls and carboxyls which can be altered or modify to produce valuable lignin-based products. Generally, modification of lignin is to synthesize new macromonomers by changing the nature of chemically active sites. There are several methods that can be applied for the production of new chemical sites in lignin structure such as hydroxyalkylation, animation, nitration, sulfomethylation and sulfonation (Laurichesse & Avérous, 2014).

1.5.2.3 Functionalization of hydroxyl group

Phenolic hydroxyl group of lignin is considered as the most reactive functional group that can modify the chemical properties of the newly formed material. The modification of hydroxyl groups can result the production of polyol derivatives of lignin. The different reaction has been used to functionalize the lignin with different functional groups such as alkylation, esterification, etherification, phenolation and urethanization (Laurichesse & Avérous, 2014).

1.5.2.4 Production of lignin graft copolymers

Lignin are used to synthesize lignin graft copolymer. Lignin graft copolymer is polymer chains attached to hydroxyl groups of lignin and form a star like branched copolymer with lignin at the centre. The lignin graft copolymer can be synthesized by two methods: (a) "grafting from" and (b) "grafting to". In "grafting from" method lignin used as a micro-initiator for the polymerization and the monomer first react with the hydroxyl group of lignin resulting polymer chain to lignin core. In "Grafting to" methods first polymer chain is synthesized that is functionalized with an end group to allow the reaction with lignin and finally grafting of the polymer chains to the lignin core by the hydroxyl groups (Laurichesse & Avérous, 2014).s

1.5.3 Application of lignin-based nanomaterials

Fabrication of lignin-based nanomaterials is in the emerging phage. Recently, researchers are interested in the production of nanomaterials and successfully produced several nanomaterials like nanoparticles, nanotubes, nanofibers and hydrogels from the lignin for different application (Figueiredo et al., 2018). Lignin nanoparticles (LNP) have several functional groups that will be modified or changed to enhance the application potential of particles. There are several methods for the production of LNP such as anti-solvent precipitation, interfacial crosslinking, polymerization solvent exchange and sonication (W. Zhao et al., 2016). Lignin based nanoparticles can be utilized in drug delivery and tissue engineering. Lignin along with other polymers is used for the synthesis of several types of hydrogel. Hydrogels are utilized for the production of contact lenses, wound dressing, drug delivery and tissue engineering

(Mishra & Wimmer, 2017). The main application of the lignin-based micro- and nanoparticles are represented in the figure 1.6.

1.5.3.1 Lignin-based nanoparticles as antioxidant

The chemical structure of lignin consists aromatic rings of the methoxy and hydroxyl groups that interact with different materials to manufacture antioxidant products, such product have several applications. These functional groups terminate the oxidative propagation reaction by releasing hydrogen (Kai et al., 2016). Lu et. al. synthesized LNPs of an approximate size of 144 nm utilizing anti-solvent precipitation methods, he uses 12.4 times higher concentration of lignin than the bulk lignin. The resulting nanoparticles manifested higher antioxidant and radical scavenging activities, that is utilized for food processing and pharmaceutical application (Q. Lu et al., 2012). Another example of antioxidant property of LNP was observed by Yearla and Padmasree, they manufacture dioxane LNPs of approximate size 104 nm using an anti-solvent precipitation method. Lignin solution was dissolved in acetone and water in ratio of 9:1 volume and the water were added. The resulting LNPs shows higher antioxidant and UV protection properties compare to the bulk lignin. Such LNPs can be useful in food, cosmetic and pharmaceutical industries (Yearla & Padmasree, 2016).

1.5.3.2 Lignin-based nanoparticles as tissue engineering

Tissue engineering is an important and emerging field of medicine. Tissue engineering can be applied for the replacing or repairing tissue to improving the function of the targeted tissue by utilizing different polymers (Furth et al., 2007). Recently, several studies prove that lignin can be used for the production of potential materials for tissue engineering such as the development of hydrogels, aerogels and nanofibers are being used for tissue engineering (Fernandes et al., 2013; Furth et al., 2007; Kai et al., 2017).

1.5.3.3 Lignin-based nanoparticles as nanocomposites

LNPs can also be used as reinforcing material in polymer matrix and nanocomposites. The resultant copolymers have enhanced biocompatibility and thermal properties compared to the original polymer. Gupta et. al. uses anti-solvent precipitation method, where lignin was first dissolved in ethylene glycol and then LNPs was precipitated by adding solvent (HCL). The fabricated LNPs was of size 181 nm, such particles were used to prepared bio-poly (trimethylene terephthalate) hybrid nanocomposites. The produced hybrid nanocomposites contain 1.5 % of LNPs and 7.0 % of vapor-grown carbon fibers by weight. Their results report an improvement in the mechanical and thermal properties of the hybrid nanocomposites (Gupta et al., 2015).

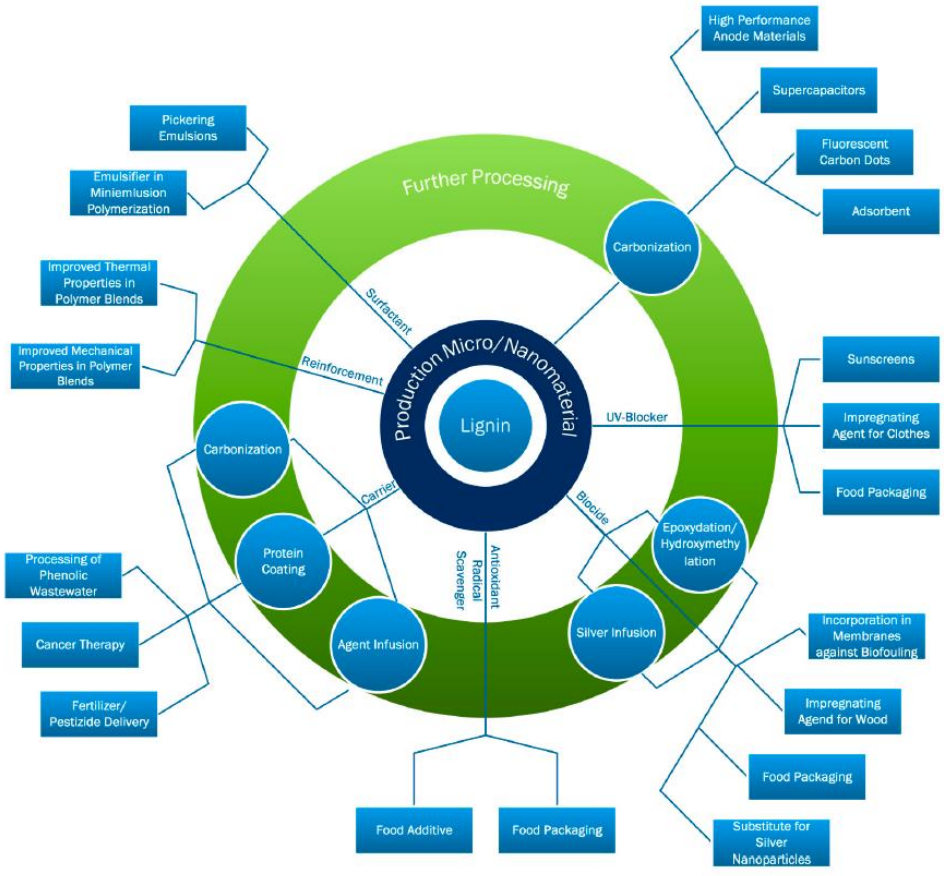

Figure 1.6 Overview of potential application of lignin-based micro- to nanoparticles. Reprinted with the permission of reference (Beisl et al., 2017).

1.5.3.4 Lignin-based nanoparticles for delivery systems

Currently, LNPs for drug delivery are most widely investigating field of application. Due to the low cost and eco-friendly properties of lignin, lignin-based nanoparticles have the potential for encapsulation of different compounds that can be used for different pharmaceutical applications. Fragville et. al. synthesized LNPs nanoparticles of size range from 100 nm to a micrometer by using anti-solvent precipitation methods. Lignin was dissolved in ethylene glycol and HCL to fabricate nanoparticles. The resulted LNPs has no cytotoxicity for yeast and microalgae. Therefore, LNPs can be consider as a good carrier for drug delivery, stabilizer of cosmetics and pharmaceutical products (Figueiredo et al., 2018; Frangville et al., 2012). Qian et. al. fabricated LNPs using self-assembly methods. The acetylated lignin was dissolved in tetrahydrofuran (THF) and the water was gradually added up to 67 % by volume of solution. Due to the hydrophobic interactions lignin molecules star to associate with each other and the nanoparticles were formed in water by the evaporation of THF. Such LNPs can be used for the drug delivery systems or microencapsulation of pesticides for target and control release (Figueiredo et al., 2018; Qian, Deng, Qiu, Li, & Yang, 2014). The hollow nanocapsules of lignin were synthesized by Yiamsawas et. al. using interfacial crosslinking methods. The obtained nanoparticles of size range from 311 to 390 nm in the water, such particles can allow to encapsulate the hydrophilic compounds like drugs, fertilizers and pesticides and can be released by enzymatic degradation of the lignin which can be used for drug delivery in agricultural application (Yiamsawas et al., 2014).

LNPs are also used for the gene delivery for human cells, Ten et. al. manufactured lignin nanotubes by using nanopore alumina membranes as a template. The resulted nanotubes show good biocompatibility and high DNA binding capacity which make nanotubes a good carrier for gene delivery into human cells (Ten et al., 2014).

Since, lignin is generated in large quantities as a by-product from pulp and paper making industries and generally burned to produce heat and electricity. Despite of the large-scale production of lignin, its utilization to produce high-value product is challenging. Recently, the production of lignin-based nanoparticles and polymers attracted the attention of researchers. Here in this project UPM, a paper mill company supply Kraft

lignin (UPM BioPiva^{TM} 395) with the aim to produce nanoparticle that can be used for different high value application. For this master thesis project, we use microfluidic platform to develop methods to fabricate nanoparticles from supplied lignin.

1.6 Aims of the study

The objective of this study is to elucidate and understand the microfluidics technology for the fabrication of lignin nanoparticles. Recently, microfluidics technique is gaining attention by researchers for the fabrication of particles. Impure kraft lignin with unknown chemical constituent is used in this project. We choose to utilize microfluidics platform for the synthesis of nanoparticles because microfluidic reaction is carried out on a microscale with fast mixing by diffusion and has the flexibility of designing microfluidic chip based on the requirement of materials. Since we know the molecular weight of lignin is high with complex chemical structure so microfluidics technique will be the suitable for fabricating nanoparticles. The specific aims of thesis are:

- Studying nanoprecipitation of lignin in different solvent systems
- Optimizing microfluidics platform for the fabrication of lignin nanoparticles
- Characterizing physiochemical properties and morphological features of lignin nanoparticles by TEM.

2. Materials and Methods

Lignin was supplied by the company called UPM and name of the lignin used for this study was kraft lignin (UPM BioPiva^{TM} 395). Microfluidics chip was design and prepared in lab, material used for the chip preparation was microscope slides (Thermo scientific), borosilicate glass capillary and Epoxy resin (Devcon 5-minute epoxy). The instrument utilized were Pump (PHD 2000, Harvard Apparatus, USA), high-speed digital microscope (Dolomite Microfluidics, UK), Zetasizer Nano series (Malvern Instruments, UK) and Transmission electron microscope (JEM-1400 plus electron microscope).

All the experiment was carried out in the lab of Pharmaceutical Science department at Åbo akademi University.

2.1 Microfluidics chip design and manufacture

Microfluidics devices used for this project was three-dimensional (3D) hydrodynamic flow focusing devices. The design of the chip was based on the solvent used for the nanoprecipitation of lignin. Microfluidics chip used for this project has 3 inlets, constructed using microscopic slides (75 X 25mm) by Thermo scientific and three borosilicate glass capillaries with diameter 2.0 mm (outer), 1.5 mm (middle) and 1.0 mm (inner). Puller model PN-31 (Narishige Japan) was used for tapering end of the borosilicate glass capillaries. Narrow borosilicate glass capillaries (1.5 mm and 1.0 mm) were pulled into a narrow size nozzle using puller. The value of main magnet, sub magnet and heater of puller for 1.0 mm capillaries were adjusted to the range of 50-52, 30-32 and 80-85 and for 1.5 capillaries adjusted to 50-52, 30-32 and 90-92 respectively to produce tapered end. Such capillaries with fine tapered end was used as inner capillaries. The thinnest inner capillary of 1.0 mm was inserted into middle capillary (1.5 mm) and finally were inserted into the outer (wider) capillary of 2.0 mm. The insertion was coaxially aligned and finally placed over glass slide and metal connectors were fixed on both ends. Out of three inlets, one receiving the fluid from inner capillary,

whereas outer and middle inlet were made by placing hypo needle (20ga) vertically over the junction between outer, middle and inner capillary. Finally, capillary was aligned over the glass slide and junctions were sealed with epoxy resin (Devcon 5-minute epoxy).

2.2 Microfluidics setup

Microfluidics chip used for this project was of two types a) microfluidics chip with two tapered end and b) microfluidics chip with one tapered end.

2.2.1 Microfluidics setup of two tapered end chip

Microfluidics used for nanoparticle fabrication consists of chips with coaxially arranged inner (1.0 mm), middle (1.5 mm) and outer (2.0mm) capillary, three pumps (PHD 2000, Harvard Apparatus, USA) and high-speed digital microscope (Dolomite Microfluidics, UK). All the three inlets (inner, middle and outer) capillaries of chip were connected with polyethylene tubes (scientific commodities INC, USA) to plastic BD syringes, these plastic BD syringes are finally connected to separate pumps (figure 2.1).

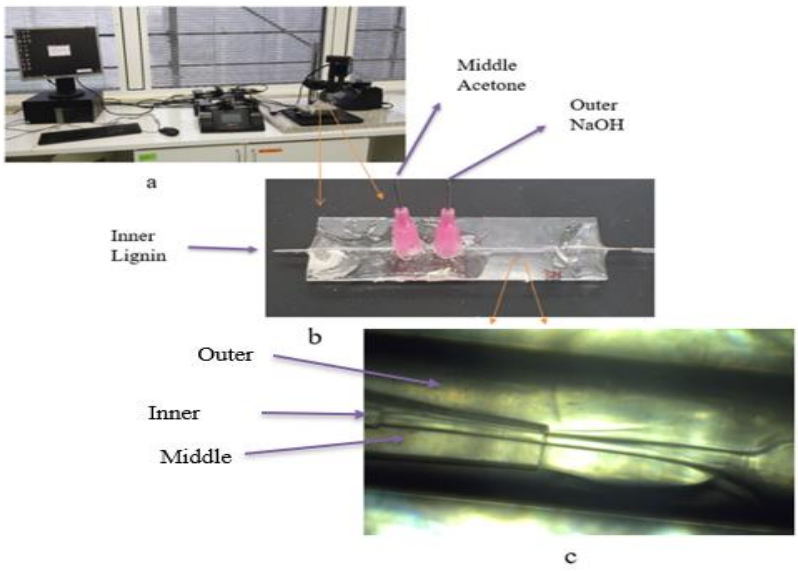

Figure 2.1 (a) Microfluidics setup consisting of Harward Apparatus USA and high-speed digital microscope. (b) 3D-HHF device with three inlets, outer inlet for NaOH, middle inlet for acetone and inner inlet for lignin. (c) High-speed digital microscope image represent capillaries are co-axially arranged and the flow pattern of fluids.

2.2.2 Final microfluidics setup

The final microfluidics design was setup for the nanoparticle fabrication consisted of two chips, microfluidics setup of two tapered end chip described in section 2.2.1 connected to microfluidics chip with one tapered end by polyethylene tube. The microfluidics chip with one tapered end consists of outer capillary of 1.5 mm with two inlets and the inner capillary of 1.0 mm. Final setup of microfluidics consists of five pumps (PHD 2000, Harvard Apparatus, USA) and high-speed digital microscope (Dolomite Microfluidics, UK). These five inlets capillaries of chips were connected with polyethylene tubes (scientific commodities INC, USA) to plastic BD syringes, these plastic BD syringes are finally connected to separate pumps. One polyethylene tube was connected from outer two tapered end chip to the inner capillary of one tapered end chip and the one polyethylene tube is connected to outlet and end in sample collecting vial (figure 2.2).

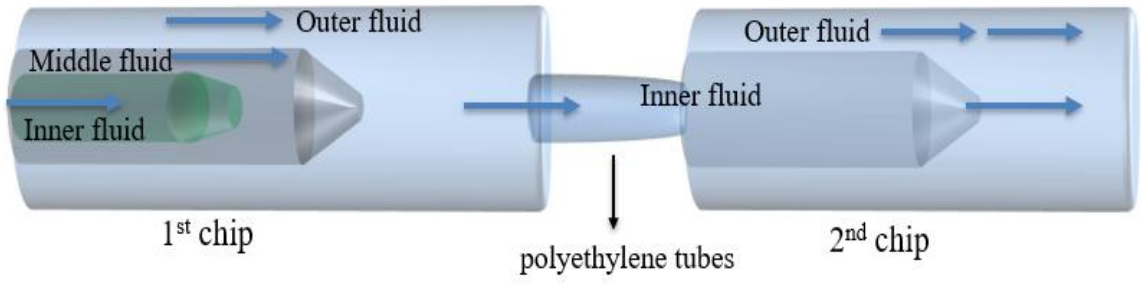

Figure 2.2 Schematic representation of final microfluidics setup consists of two chips connected via polyethylene tune. Two tapered end chip contains three capillaries and three inlets, outer inlet for NaOH (outer fluid), middle inlet for acetone (middle fluid) and inner inlet for lignin (inner fluid). One tapered end chip consists of two capillaries with three inlets, outer inlet for NaOH and acetone (outer fluid) and solution obtain from two tapered end chip pass through the inner inlet (inner fluid) of one tapered end chip.

2.3 Sample preparation and nanoparticles fabrication

Lignin was dissolved in ethylene glycol by sonicating and alternative vertexing for approximately for 15 minutes to ensure that the lignin was completely solubilized. Solvents used for the nanoprecipitation was NaOH (0.1 M) and pure acetone. For two tapered end chip, solvent used for the precipitating lignin was NaOH (0.1 M) in outer capillary, pure acetone in middle capillary. Three different syringe of 30 ml containing lignin (0.1%), acetone and NaOH (0.1 M) were fixed with clamps of pumps. Syringes were connected to inner, middle and outer capillary inlet of 3D-HFF microfluidics device via polyethylene tubes (Scientific Commodities INC, USA). Pumps was used to control and monitor the flow rate of fluids. Different flow rate ratios (FRR) were investigated to find the optimum flow rate for the nanoprecipitation.

2.3.1 Flow rate optimization of two tapered end chip

The flow rates of inner inlet i.e. lignin (0.1 %) was kept constant 2 ml/hr whereas flow rates of middle inlet (acetone) and outer inlet (NaOH 0.1 M) were altered to ensure the compatibility of result, each experiment were perform three round of sample collection. First sample was collected at the flow rate ratio (FRR) of 2:20:0.5 ml/hr (lignin: 2ml/hour, acetone:20 ml/hour and NaOH:0.5 ml/hour), followed by different FRR such as 2:20:1 ml/hr, and 2:20:2 ml/hr. Optimized flow rate of two tapered end chip was determined by examine different flow rate ratio of solvents, presented in table 2. All the sample were collected from the outlet channel in separate glass vails (4ml) via polyethylene tube.

Table 2. The different flow rate of solvents was analysed to derive the optimized flow rate of microfluidics chip with two tapered ends.

Solvent	Lignin (0.1%) (Inner inlet)	Acetone (pure) (Middle inlet)	NaOH (0.1 M) (Outer inlet)
Flow rate (ml/hr)	2	40	2
Flow rate (ml/hr)	2	20	2
Flow rate (ml/hr)	2	20	1
Flow rate (ml/hr)	2	20	0.5
Flow rate (ml/hr)	2	10	2
Flow rate (ml/hr)	2	10	0.5

2.3.2 Flow rate optimization of one tapered end chip

For microfluidics chip with one tapered end, solvent NaOH (0.1 M) and pure acetone was used in the outer capillary and the solution obtain from the microfluidics chip with two tapered ends was transferred directly to the inner capillary of one tapered end chip for nanoprecipitation of lignin. Two different syringes of 30 ml containing NaOH (0.1 M) and acetone were fixed with clamps of pumps. Syringes were connected to outer capillary inlet of microfluidics chip via polyethylene tubes (Scientific Commodities INC, USA). A polyethylene tube was used to connect the outlet of two tapered ends chip to the inner capillary of one tapered end chip. Pumps was used to control the flow rate of fluids. The different flow rate ratio was analysed to determine the optimum flow rate (table 3).

The flow rates of inner inlet i.e. the solution flow from outlet of two tapered end chip, represented as (SOL1) and one of the outer inlet solvent acetone (20 ml/hr) were kept constant whereas the flow rates of another outer solvent NaOH (0.1 M) was raised in ascending order 1.0 ml/hr, 2 ml/hr, 3 ml/hr and 4 ml/hr during experiment. To ensure the compatibility of result, each experiment perform three round of sample collection. First sample was collected at the FRR of SOL1:20:1 ml/hr (SOL1 means solution flow directly from two tapered end chip with flow rate of 23 ml/hr, 20 is acetone and 1is NaOH flow rate), SOL1:20:2 ml/hr, SOL1:20:3 ml/hr and SOL1:20:4 ml/hr. All the different FRR sample were collected from the outlet channel in separate glass vails (4ml) via polyethylene tube. The collected sample were immediately evaluated with Zetasizer Nano series (Malvern Instruments, UK) for the size distribution and zeta potential.

Table 3. Represent different flow rate of solvents that was analysed to determine the optimum flow rate ratio of one tapered end chip.

Solvent	SOL1 (inner inlet)	Acetone (pure) (outer inlet)	NaOH (0.1 M) (Outer inlet)
Flow rate (ml/hr)	23	20	1
Flow rate (ml/hr)	23	20	2
Flow rate (ml/hr)	23	20	3
Flow rate (ml/hr)	23	20	4

SOL1: optimized solution flow directly from outlet of two tapered end chip to inner inlet of one tapered chip.

Cautions:

Bubble formation should be avoided while filling the lignin and solvent solution in syringe. Bubbles formation in the syringe can cause disturb to the fluid flow and affect the nanoprecipitation process.

Troubleshooting:

Bubbles formation can be avoided by tapping syringe gently with a finger and by pressing the plunger to remove bubbles out of the syringe.

2.4 Characterization and evaluation of nanoparticles

Primary characterization and evaluation of nanoparticles was done with Zetasizer Nano series (Malvern Instruments, UK). Nanoparticles size and PDI were measured by dynamic light scattering (DLS) with Zetasizer. For size and PDI measurement, 1 ml of the diluted sample (30 µl of nanoprecipitate sample were dissolved in 1 ml milli-Q water) were loaded in disposable polystyrene cuvette (VWR® cuvettes PS, USA). While to measure the zeta-potential same instrument (Zetasizer Nano series) were used, 1 ml of diluted sample (30 µl of nanoprecipitate sample were dissolved in 1 ml of HEPES buffer with pH value 7 were loaded in disposable folded capillary cell (DTS1070, Malvern Instruments, UK).The presented results are the average of three measurement of each FRR.

2.4.1 Dynamic light scattering and zeta potential

Dynamic light scattering (DLS) also known as photon correlation spectroscopy or quasi-elastic light scattering, is techniques used to measure the hydrodynamic size and surface charge of the nanoparticles by calculation of diffusion coefficient of polymeric solution (Stetefeld, McKenna, & Patel, 2016). Nanoparticles are in continuous Brownian motion in solution. The charge surface of the nanoparticles generates complex interaction between ions and molecules. Which generate layer of adsorbed ions on to the charged surface of nanoparticles. These properties of colloidal dispersion are used by DLS and zeta potential to calculate hydrodynamic size and potential difference.

2.4.1.1 Principle of DLS

DLS measures the hydrodynamic size of the nanoparticles by detecting the scattering from laser that passes through colloidal solution. The light energy depends on the particles motion, if the particles are stable light energy remain constant. When the particles are in continuous motion, change in energy of scattering light is observed due to constructive and destructive interferences. These fluctuating intensities is used to determine diffusion coefficient of particles to evaluate their Brownian motion utilizing Stockes-Einstein equation is presented below.

$$D_t = \frac{k_B T}{6\,\pi\eta R_H}$$

Where D_t is diffusion coefficient, K_B is Boltzmann constant (1.38064852 x 10^{-23} J/K), T is temperature, η is absolute viscosity and R_H is hydrodynamic radius. The result of the DLS depends on the viscosity of solvent, instrument, temperature and the refractive index of the material radius. Here, in this project Zetasizer Nano ZS was used to determine the hydrodynamic size of the nanoparticles. Particle size was represented as size distribution curve and PDI reflects the width of particle size distribution by calculating $(\text{width/mean})^2$ of each peak. PDI value less than 0.2 usually represents monodisperse particles and value above 0.2 represent polydisperse particles. The DLS gives a primary idea about the size of nanoparticles but it does not measure the original size of the synthesized nanoparticles. Sample concentration can affect the measurement

of the particles size. At the higher concentration of sample, multi-scattering causes the interaction among the scattered light of other particles resulting in loss of intensity and gives small size reading in comparison to the original. While in very diluted concentration light scattering is not effective. There is no any standard concentration for optimum size of particles. There are different factors such as scattering volume, laser power, length of scattering, detector sensitivity and material properties can affect the optimum concentration. In practice optimum concentration can be set for particular material by screening the serial dilution to determine the optimum concentration (Bhattacharjee, 2016; Stetefeld et al., 2016).

2.4.1.2 Zeta potential

Zeta potential or electrokinetic potential can define as "the potential at the slipping/shear plane of colloid particle moving under electric field"(Bhattacharjee, 2016). Zeta in Greek letter denoted as ζ, hence also called as ζ-potential. Zeta potential describe the potential difference between the electric double layer and the dispersion medium at the slipping plane (figure 2.3).

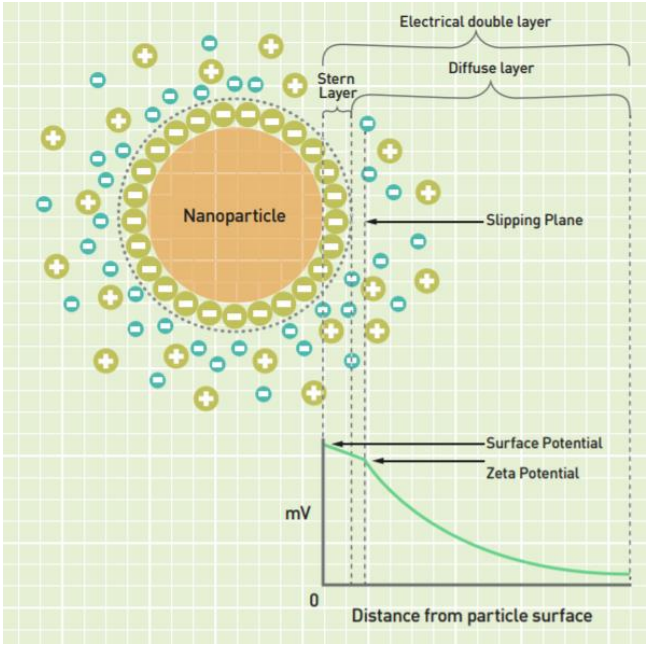

Figure 2.3 Diagram represented ionic concentration and potential difference as a function of distance from the nanoparticle surface. Electrical double layer of nanoparticle consists of inner stern layer and outer diffuse layer. In Stern layer ions are bound strongly and in diffuse layer ions are bound less firmly. The potential difference between the double layer and the dispersion medium is zeta potential. Figure obtain from the Malvern Instrument website: https://www.malvernpanalytical.com/en/assets/MRK1839_tcm50-17228.pdf

The surface of the nanoparticles consists of double layer, inner Stern layer contains opposite charged ion at the particle surface. The outer diffuse layer composed of both opposite and the same charged ion. These both layers are referred as an electrical double layer. The slipping plane is form with in the diffuse layer due to the movement of charged particles towards the opposite electrode in the electric field and it is used to calculate the zeta potential.

To measure zeta potential first the electrophoresis mobility (μ_e) of particles are to be calculated as given in equation below.

$$\mu_e = \frac{V}{E}$$

Where V is particular velocity (μm/s) and E is electric field strength (Volt/cm).

Now zeta potential can be calculated using the value of μ_e in the Henery's equation.

$$\mu_e = \frac{2\varepsilon_r \varepsilon_0 \zeta f(ka)}{3\eta}$$

Where $\varepsilon_r$is relative permittivity/dielectric constant, ε_0 is permittivity of vacuum, ζ is zeta potential, $f(ka)$ is Henry's function and η is viscosity at experimental temperature (Bhattacharjee, 2016).

There are several factors that influence the zeta potential measurement such as pH and ionic strength. Depending upon the surface charge of particle the zeta potential can be either positive or negative. Hence, at particular pH zeta potential can be reached to isoelectric point where zeta potential of particle became zero, it is also called point of zero charge (PZC). The loss of isoelectric repulsion causes colloidal dispersion unstable resulting in flocculation or agglomeration. Ionic strength affects the zeta potential by influencing the compactness of electric double layer. With increasing ionic strength, zeta potential decreases by compressing electric double layer and vice versa. Zeta potential here in this experiment mainly use to evaluate the surface charge of the nanoparticles. Another main purpose of zeta potential measurement was to get information about the colloidal dispersion stability. The colloidal dispersion stability can be explained by theory called DLVO theory that state the sum of Van der Waal forces and electrostatic

repulsive forces are mainly responsible for stability. The colloidal dispersion stability can be classified as highly unstable, relatively stable, moderately stable and highly stable based on zeta potential value ±0-10, ±10-20, ±20-30 and ≥±30 respectively (Bhattacharjee, 2016; Missana & Adell, 2000).

2.5 Morphological analysis of nanoparticles

Further, Transmission electron microscopy (TEM; JEM-1400 Plus Electron Microscope, JEOL, Japan) were used to confirm the result of DLS and zeta-potential. TEM were used for the morphological analysis of nanoparticles.

To prepare the TEM sample, particles obtain from the microfluidics outlet were transferred to Eppendorf and centrifuged (LaboGene, Denmark) at 13 rpm for 8 min. Pellets collected was washed once with different solvents and then re-dispersed in 1 ml of same solvent. List of solvents used for washing are presented in table 4. The sample were properly mixed by vortexed and sonicated before 10 µl of dispersed sample was dropped on the carbon-coated grid (Ted Pella Inc., USA). The grid was left for overnight for drying.

Table 4. List of solvents used for washing nanoprecipitate.

Solvents
Acetone
Ethanol
HCL
Water

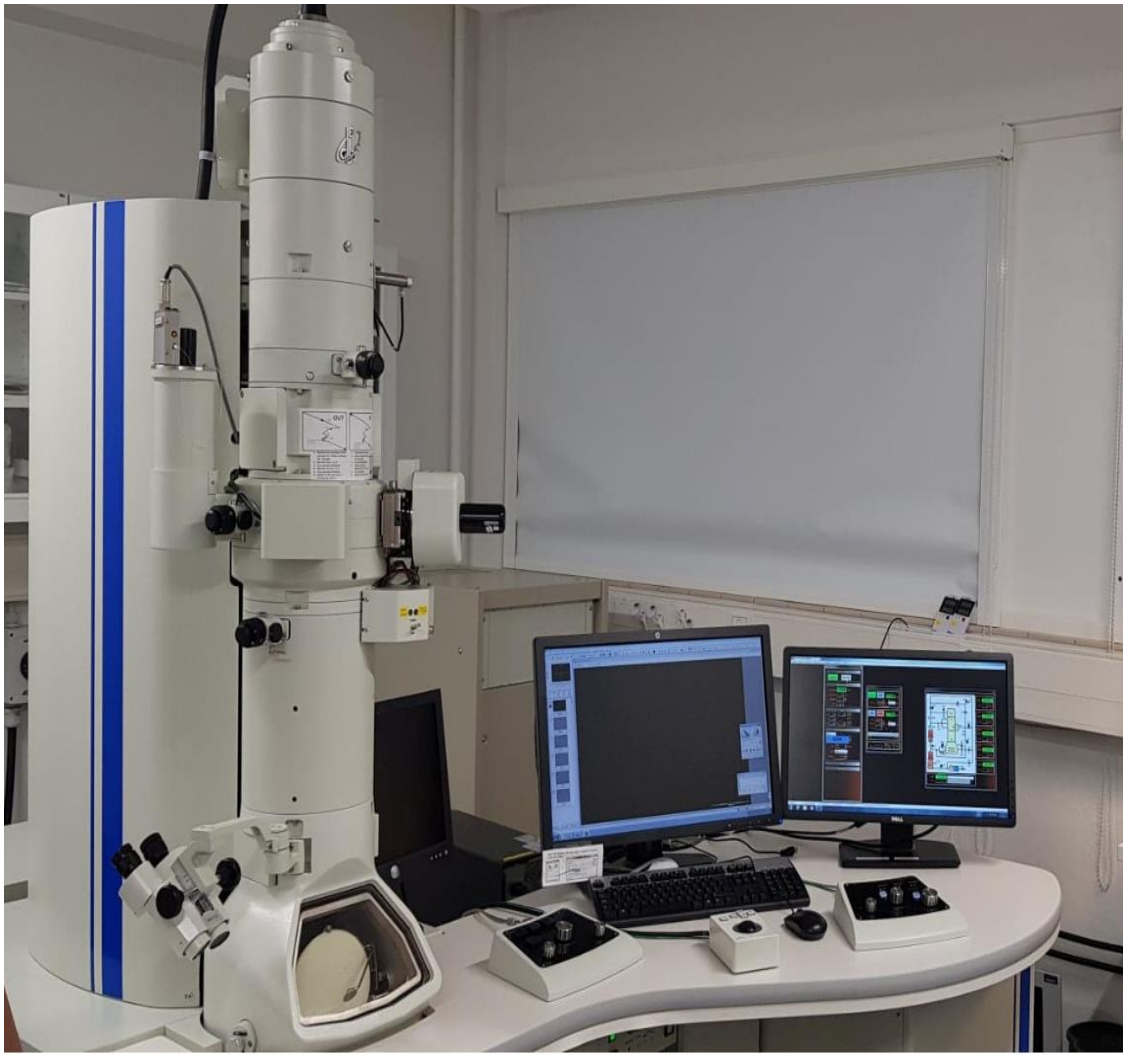

Figure 2.4 Transmission electron microscope used for the morphological analysis of nanoparticles. JEM-1400 Plus Electron Microscope (JEOL, Japan).

TEM principle is based on the penetration of electrons through a sample or specimen. For the imaging, TEM uses different type of lenses to form a transmission electron diffraction pattern and the image magnification in the range of 10^3 to 10^6 can be obtained. To understand the mechanism of TEM, the instrument can be classified into three parts: a) Illumination systems, b) specimen stage and c) imaging systems. Illumination systems consist of the electron gun, the electron gun in JEM-1400 electron microscope comprises of a V-shaped crystal fabricated of lanthanum hexaboride (LaB6) (R. F. Egerton, 2016).

A beam of electron is generated when the current passes through V-shaped crystal of LaB6 heats the tip of crystal to 1800k to emits electron under vacuum condition is called thermion emission. Such emitted electron is accelerated through an electric field and focus on the sample by two different condenser lenses. Nowadays, mostly lenses used for the electron beam are electromagnetic lenses. In the specimen stage, pre-prepared copper grip is placed on a small circular hole at the tip of sample holder. The sample holder is inserted into the side-entry stage of the vacuum TEM column through airlock. Finally, the imaging systems produce magnified images using a series of lenses. The operating voltage used in JEM-1400 Plus Electron Microscope was 80KV, which result resolution of 10 nm. There are several other advanced electron microscopes that can use high accelerating voltage such as 200KV, 100KV and produce resolution of 0.2 nm and 0.3 nm (Ray F. Egerton, 2005). To get well resolved image, working panel equipped with the control system to adjust magnification, focus and brightness. Generally, image was taken with magnification of 8000x, 20000x and 200000x to get pictures of size of scale 1μm, 200nm and 50nm.

3. Results

Kraft lignin (UPM BioPiva^{TM} 395) supplied by UPM, was used in this project for fabricating nanoparticles with microfluidics technology. Lignin was dissolved in ethylene glycol whereas NaOH was used for triggering precipitation and acetone as a counter solvent.

The overall results of this project can be explained in two major parts: first one is optimizing flow rate ratio (FRR) of two tapered end microfluidics chip and second one is optimizing FRR of one tapered end microfluidics chip for sequential precipitation.

3.1 Optimizing FRR of two tapered end microfluidics chip

Design of the microfluidic chip is described in section 2.2. We design such type of microfluidics chip because we were unable to precipitate the lignin with one solvent. Based on the literature we know that the chemical structure of lignin is a complex and it has different functional group such as methoxy, carboxylic, carbonyl, phenolic and aliphatic hydroxy. Since, lignin structure have different functional group. We hypothesized that if we introduce NaOH in addition to acetone so that NaOH will ionize acids presented in lignin and will trigger the precipitation. As the lignin used in this project is impure and we do not have knowledge about its chemical characterization. Based on this hypothesis we design the microfluidic chip, consist of three inlets with two tapered ends, from inner inlet lignin (0.1%), middle inlet acetone and outer inlet NaOH (0.1 M) were supplied.

The flow rate of used solvents in this project were varied in different order to investigate how flow rate of solvents affect the physicochemical properties such as particles size and distribution of fabricated lignin nanoparticles. To optimization of FRR for nanoprecipitation three set of experiment were performed with different sets of solvents FRR.

3.1.1 Optimizing acetone infusion rate on nanoparticles fabrication

Acetone was used as counter solvent; we select acetone as counter solvent for this project because we used impure lignin with unknown chemical characteristic. Therefore, we must select such solvent which have ability to dissolve both polar and nonpolar substance. NaOH was used for triggering precipitation by ionizing acid present in lignin. Ethylene glycol were used to dissolve lignin and 0.1% of lignin was used in this project. The flow rate of lignin (0.1%) were always kept constant at 2 ml/hr because we used impure lignin and lignin have high molecular weight, ranging from 1000 to 50000 g/mol (see table 1). Hence, we kept lignin flow rate constant and we changed FRR of other solvents to optimized nanoprecipitation.

To optimize the nanoparticle fabrication, at first flow rate of inner fluid lignin (0.1%) and the outer fluid NaOH (0.1 M) were kept constant at 2 ml/hr whereas middle fluid acetone volume varied in ascending order 10, 20 and 40 ml/hr. Hence, three different flow rate ratio (FRR) 2:10:2 ml/hr (2 ml/hr lignin: 10 ml/hr acetone: 2 ml/hr NaOH), 2:20:2 and 2:40:2 ml/hr was evaluated to determine optimum conditions for the nanoparticles fabrication, results presented in figure 3.1.

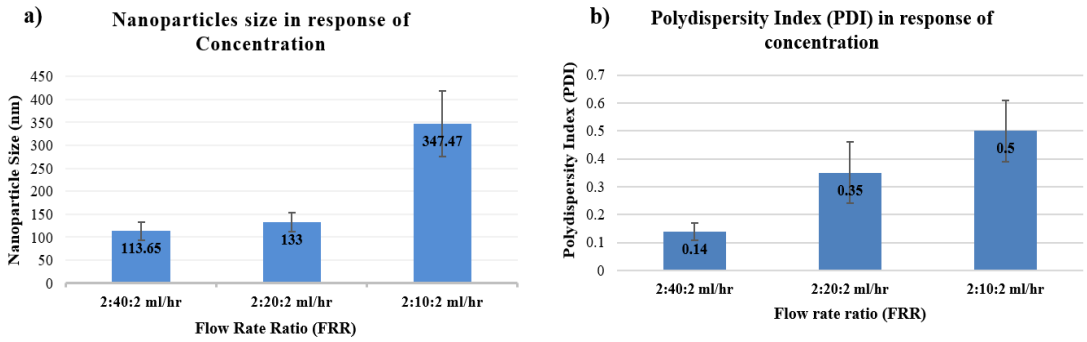

Figure 3.1 a) Average hydrodynamic nanoparticle size of lignin in response of different flow rate ratio (FRR) measured with Zetasizer Nano ZS. b) Corresponding polydispersity index (PDI) in response of different FRR measured with Zetasizer Nano ZS. Standard deviation was presented in both diagrams.

Following results were derived from this experiment, it was observed that the particle size was tunable with the changes in the flow rate of acetone. The particle size and

polydispersity index (DPI) were increased with decreasing FRR of the acetone. Particles with hydrodynamic size of 113.65±19.54 nm and PDI 0.14±0.03 at the highest FRR (i.e. 2:40:2 ml/hr) were observed. Whereas, particle size increased to 347.47±71.19 nm and PDI 0.5±0.11at the lowest flow rate of acetone (2:10:2 ml/hr) used in the study. It is obvious to increase the size of the particles with decreasing flow rate of acetone. As we know at low Reynold number, (i.e. high inertial force) the central stream is squeezed into a narrow steam between two adjacent streams. Such narrow width stream causes rapid mixing by diffusion. If mixing occur faster than the time scale for aggregation of nanoparticles, size of the particles expected to be small and more homogeneous than the particles prepared at slow mixing. Here in this experiment high flow rate of acetone generate rapid mixing time compare to the low flow rate of acetone. Hence the size of the particle increased with decreasing flow rate of acetone. Particles were easily tunned from 113.65±19.54 nm to 347.47±71.19 nm by successively decreasing flow rate of acetone from 40 ml/hr to 10 ml/hr.

3.1.2 Effect of acetone and NaOH flow rate on nanoparticle fabrication

The flow rate of inner fluid (lignin 0.1%) was kept constant (2 ml/hr) and in contrast the flow rate of middle (acetone) and outer (NaOH 0.1 M) fluids was varied to optimize lignin nanoprecipitation. Hence, following flow rate were studied i.e. 2:40:2 ml/hr (i.e. 2 ml/hr of lignin: 40 of acetone: 2 ml/hr of NaOH), 2:20:1 and 2:10:0.5 ml/hr. Result obtained from Zetasizer Nano ZS are represented in figure 3.2.

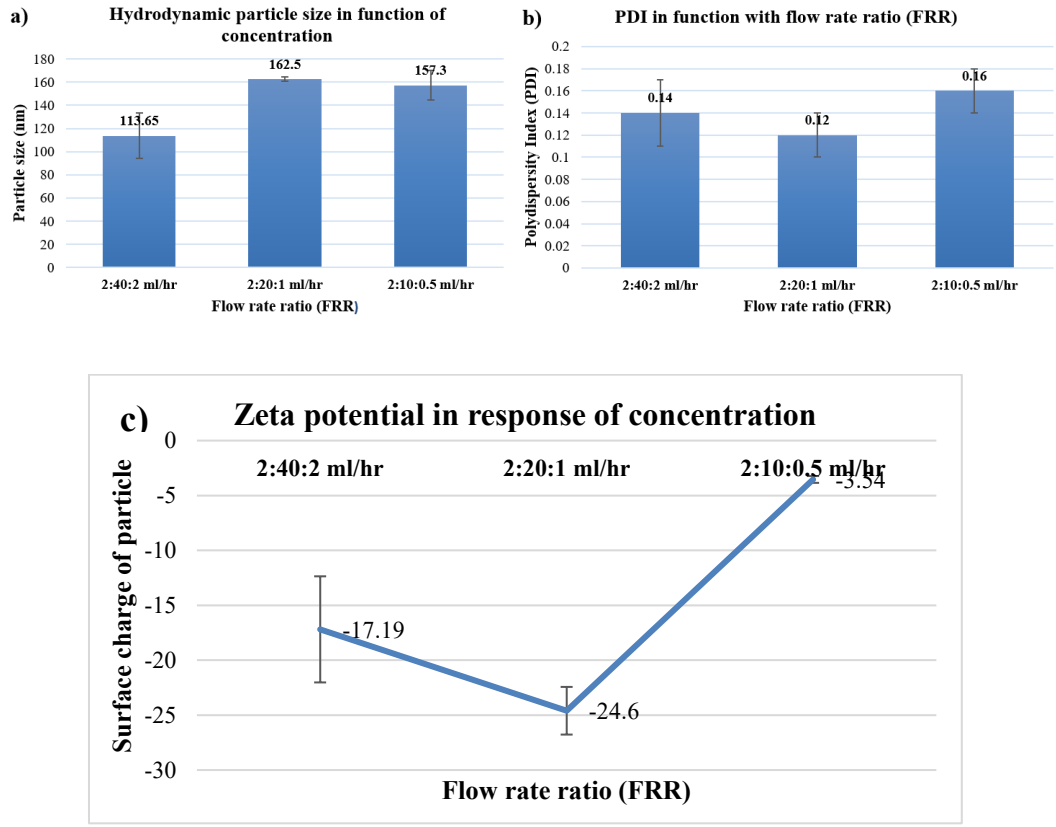

Figure 3.2 a) Average hydrodynamic nanoparticle size of lignin in function with different flow rate ratio (FRR). b) Corresponding polydispersity index (PDI) in response of different FRR and c) zeta potential of nanoparticle measured with Zetasizer Nano ZS. Standard deviation is presented in the diagrams.

The second series of optimization was conducted by manipulating both flow rate of acetone and NaOH. Subsequently particles were collected and particles size and zeta potential were analysed with zetasized Nano ZS. Optimization was started with high acetone and NaOH flow rate i.e. 2:40:2 ml/hr and gradually decreased to 2:20:1 and 2:10:0.5 ml/hr. At the FRR of 2:40:2 ml/hr, size of the particles was 113±19.54 nm, PDI 0.14±0.03 and zeta potential -17.19±4.83 mV and the size of particles increased to 162.5±1.82 nm, PDI and zeta potential decreased to 0.12±0.02 and -24.6±2.17 mV respectively at FRR of 2:20:1 ml/hr. Whereas, size of the particles decreased to 157.3±12.68 nm, PDI and zeta potential increased to 0.16±0.02 and -3.54±0.31 respectively at the FRR 2:10:0.5. Based on the hydrodynamic size, PDI and zeta potential value FRR 2:20:1 ml/hr consider as optimal flow rate. Generally, PDI value less than 0.2 consider as monodispersed particles and zeta potential in the range of ±20-30 is considered as the colloidal dispersion stability of particles is moderately stable.

3.1.3 Optimizing NaOH infusion rate on nanoparticles fabrication

Following the results mentioned in section 3.1.2, experiment was set by changes in the flow rate of outer fluid NaOH in ascending order as 0.5, 1.0 and 2.0 ml/hr to ensure the effect of NaOH on nanoparticles fabrication and also to find the optimum concentration of NaOH for ionization of acid that might be present in the lignin. Therefore, the experiment was set with FRR as 2:20:0.5 (2 is lignin, 20 is acetone and 0.5 is NaOH), 2:20:1 and 2:20:2 ml/hr. The results derived from Zetasizer Nano ZS were presented in figure 3.3.

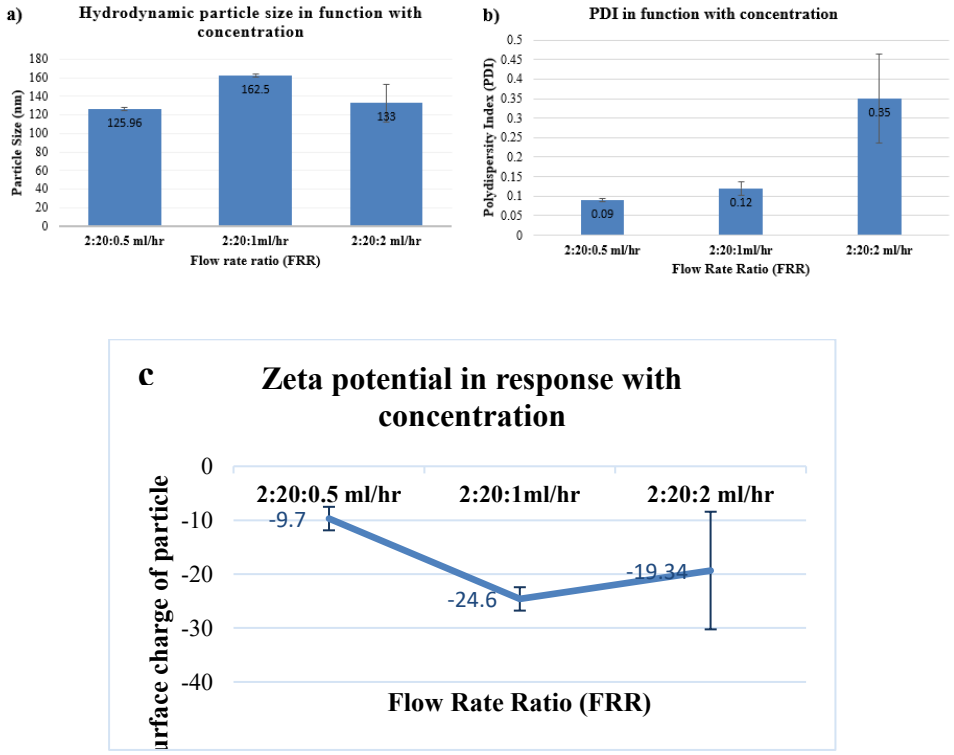

Figure 3.3 a) Average hydrodynamic nanoparticle size of lignin in function with different flow rate ratio (FRR). b) Corresponding polydispersity index (PDI) in response of different FRR and c) zeta potential of nanoparticle were measured with Zetasizer Nano ZS. Standard deviation is presented for each value in the diagrams.

The hydrodynamic size of the particles at FRR 2:20:0.5 ml/hr was 125.96±1.68 nm, corresponding PDI 0.09±0.004 and the zeta potential -9.7±2.18 mV, size of the particles was increased to 162.5±1.82 nm, PDI increased to 0.12±0.017 and zeta potential decreased to -24.6±2.17 mV at FRR 2:20:1 ml/hr. While the size of particles decreased to 133±20.42 nm, PDI and zeta potential increased to 0.35±0.11 and -19.6±10.91 mV at FRR of 2:20:2 ml/hr. The results obtained from this experiment conclude that the FRR 2:20:1 ml/hr was the optimal flow rate based on the size, PDI and zeta potential value for the nanoprecipitation of nanoparticles.

3.1.4 Morphological analysis of nanoparticles by TEM

The optimized FRR (2:20:1 ml/hr) was selected for the nanoprecipitation and TEM image analysis of lignin nanoparticles. Nanoprecipitate of stock sample obtain by microfluidics were analyzed with TEM. Carbon-coated grid were prepared for TEM image analysis, preparation of carbon-coated grid was described in section 2.5.

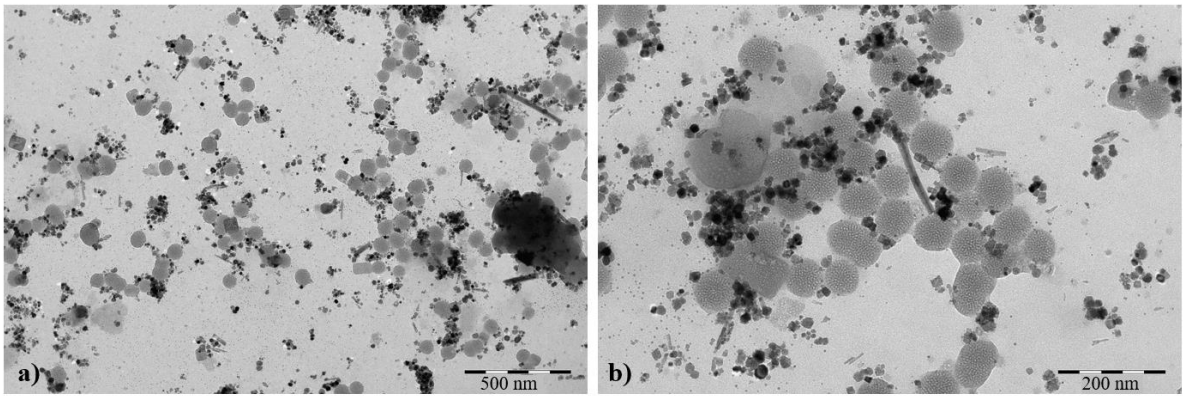

Figure 3.4 TEM image of lignin nanoparticles derived by microfluidics at optimized FRR of stock solution. Scale bar: a) 500 nm and b) 200 nm.

TEM image of stock sample presented in figure 3.4 shows different types of particles. We observed at least three different nanoparticles, first porous nanoparticles (average size from 50 to 80 nm), nonporous particles and dark nanocrystals. Hence, interested and focused on purification of nanoparticles especially porous particles as there are no reports on synthesis of porous nanoparticles from lignin material.

3.1.4.1 Purification and morphological analysis of lignin nanoparticles

The nanoprecipitate derived utilizing microfluidics technique were washed with different solvents and carbon-coated grid were prepared for TEM image analysis. Purification of nanoprecipitate were conducted with single solvent system and sequential washing systems by using different solvents (table 5).

Table 5. Represent different purification systems of nanoprecipitate and resulted types of nanoparticles by TEM.

Single solvent system	
Solvent	**Nanoparticles types**
Acetone	Porous and spherical
Ethanol	Solid and spherical
HCL	Porous and spherical
Water	Porous and spherical
Sequential washing system	
Acetone-ethanol	Solid and spherical
Acetone-ethanol-HCL	Solid and spherical

Since the chemical composition of lignin is unknow we must have to select appropriate solvent for washing nanoprecipitate. Therefore, we decide to wash the nanoprecipitate with different type of solvents such as acetone, ethanol, HCL and water. These solvents have different properties: acetone has ability to dissolve both polar and nonpolar substances, ethanol dissolve nonpolar substances, HCL is excellent solvent for metal oxide and metals and water is consider as universal solvent as it dissolves more

substance than other liquid. Sequential washing was performed with the possibility of removing nonporous and nanocrystal the solution. Sequential washing systems uses acetone, ethanol and HCL, for sequential washing nanoprecipitate was first washed with acetone and the remaining precipitate was washed with ethanol. Likewise, nanoprecipitate washed with acetone and remaining precipitate washed with ethanol and finally remaining precipitate with HCL. The TEM results derived after washing nanoprecipitate is presented in figure 3.5.

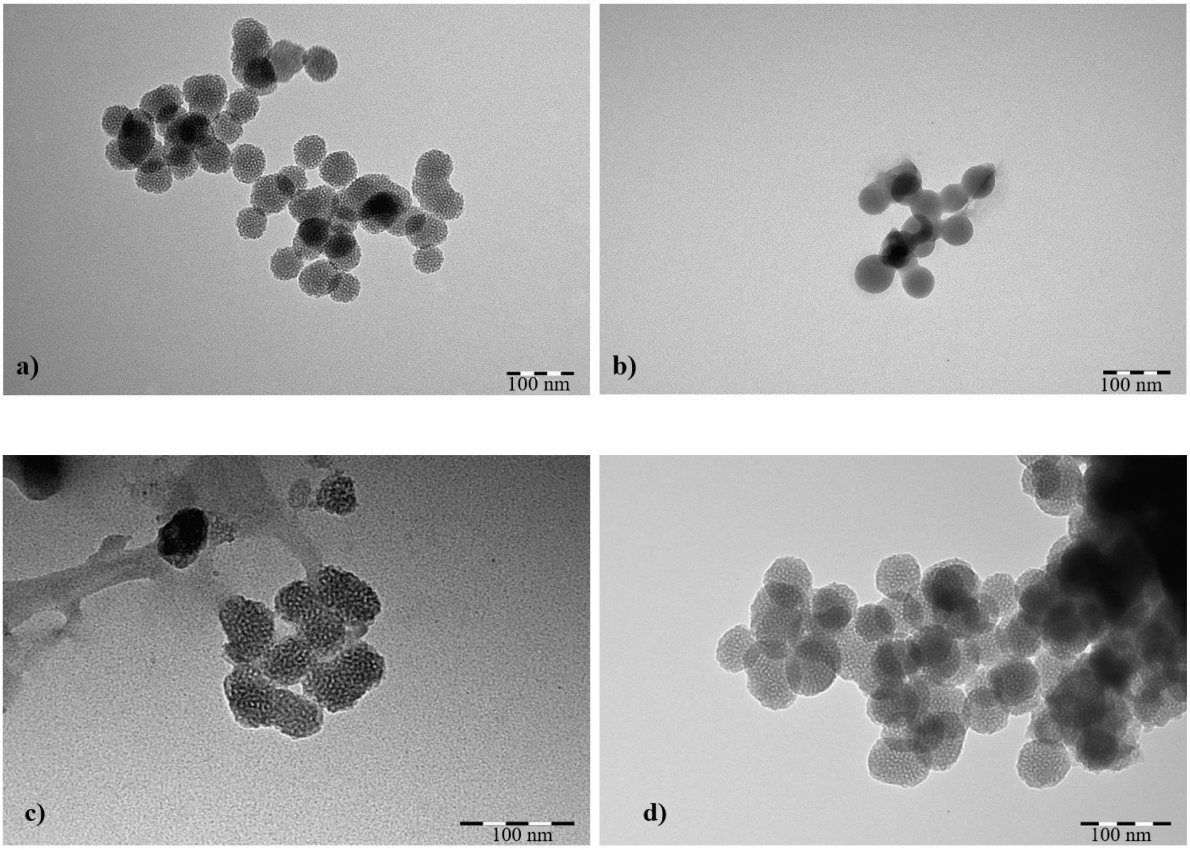

Figure 3.5 TEM image of lignin nanoparticles washed with different solvents a) washed with acetone, scale bar 100 nm, b) washed with ethanol, scale bar 100 nm, c) washed with HCL, d) washed with water, scale bar: 100 nm.

TEM image represented the morphological characterization of fabricated nanoparticles, it was observed that the nanoparticles derived after the washing with solvents acetone, HCL and water was porous nanoparticle, while nanoparticle obtained by washing with ethanol was solid spherical nanoparticles presented in figure above. The average size of fabricated nanoparticle was in the range of 50 to 80 nm in diameter. TEM image of sequential washing is presented in figure 3.6.

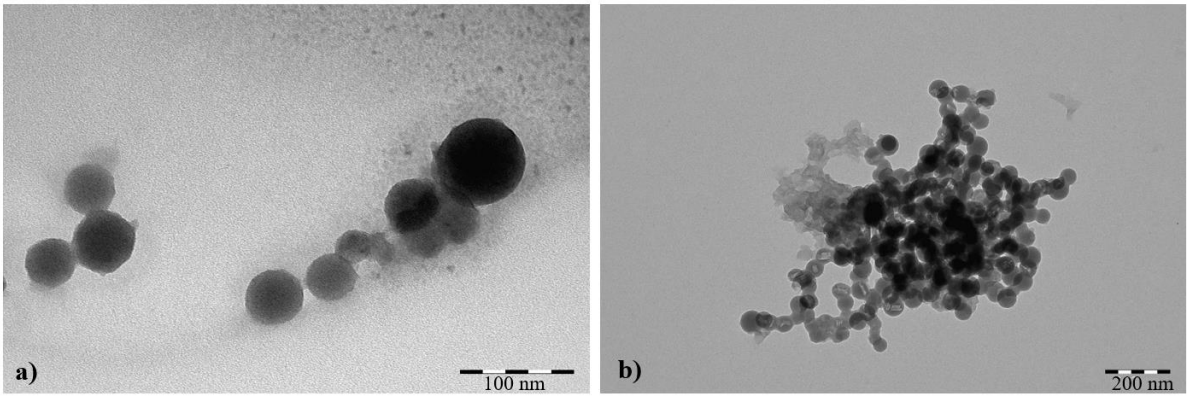

Figure 3.6 TEM image of lignin nanoparticles washed with different solvents by sequential precipitation a) washed with acetone and remaining precipitate was wash with ethanol, scale bar: 100 nm and b) washed with acetone and remaining precipitate was washed with ethanol and finally remaining precipitate washed with HCL, scale bar: 200 nm.

TEM result shows the nanoparticles derived after the sequential washing are of solid and spherical structure. The average size of derived nanoparticles is in the range of same as it was obtained by washing individual solvents. Unfortunately, the results presented in figure 3.5 and 3.6 were not reproducible but we able to obtain few porous nanoparticles in some of the repeated experiments.

3.2 Optimization for sequential precipitation

Following the results mention in section 3.1.4 and discussion with the supervisor, it was suggested that the porous nanoparticles may presented in the lignin but might be in small quantity or it might be of hybrid nature. Lignin used in this project was impure and its chemical constituent is not characterised but based on the literature we know that the lignin is complex organic polymer which is composed by three phenylpropane monomers. Lignin monomers are covalently interconnected with different linkage such as C-C (condensed bonds) and C-O-C (ether bonds), β-O-4, 5-5, β-5, 4-O-5, β-1,

dibenzodioxocin and β- β to form polymer. Since the chemical structure of lignin is complex and link with several linkage that might be the reason, we do not able to nanoprecipitate those porous or hybrid particles. Therefore, we decided to use sequential precipitation to overcome this problem. Two microfluidic chips were utilized for the sequential precipitation of nanoparticles. The microfluidics chip and the optimum flow rate of two tapered end chip kept the same as it was described in section 3.1.3. Second chip was designed having three inlets with one tapered end, the schematic representation of experimental setup was represented in figure 2.2.2.

3.2.1 Optimization of flow rate for hybrid nanoparticles fabrication

The optimum flow rate (2:20:1ml/hr) of two tapered end chip was kept constant as it was already optimized by several experiment (see section 3.1) and for the one tapered end chip the inner fluid (solution directly transfer from two tapered end chip outlet to one tapered end chip inner inlet is represented as SOL1) and one of the outer fluid acetone (20 ml/hr) were kept constant and the another outer fluid NaOH (0.1 M) were varied in ascending order from 1, 2, 3 and 4 ml/hr. Therefore, the flow rate was represented as SOL1:20:1 ml/hr, where SOL1 is solution directly transferred at the rate of 23 ml/hr from two tapered end chip outlet to inner inlet of one tapered end chip, 20 ml/hr is the flow rate of acetone and 1ml/hr is flow rate of NaOH (0.1M) in outer inlet of one tapered end chip. Hence, following flow rates: SOL1:20:2 ml/hr, SOL1:20:3 ml/hr and SOL1:20:4 ml/hr were used to optimized the synthesis of hybrid nanoparticles. The result acquired from Zetasizer Nano ZS were presented in figure 3.7.

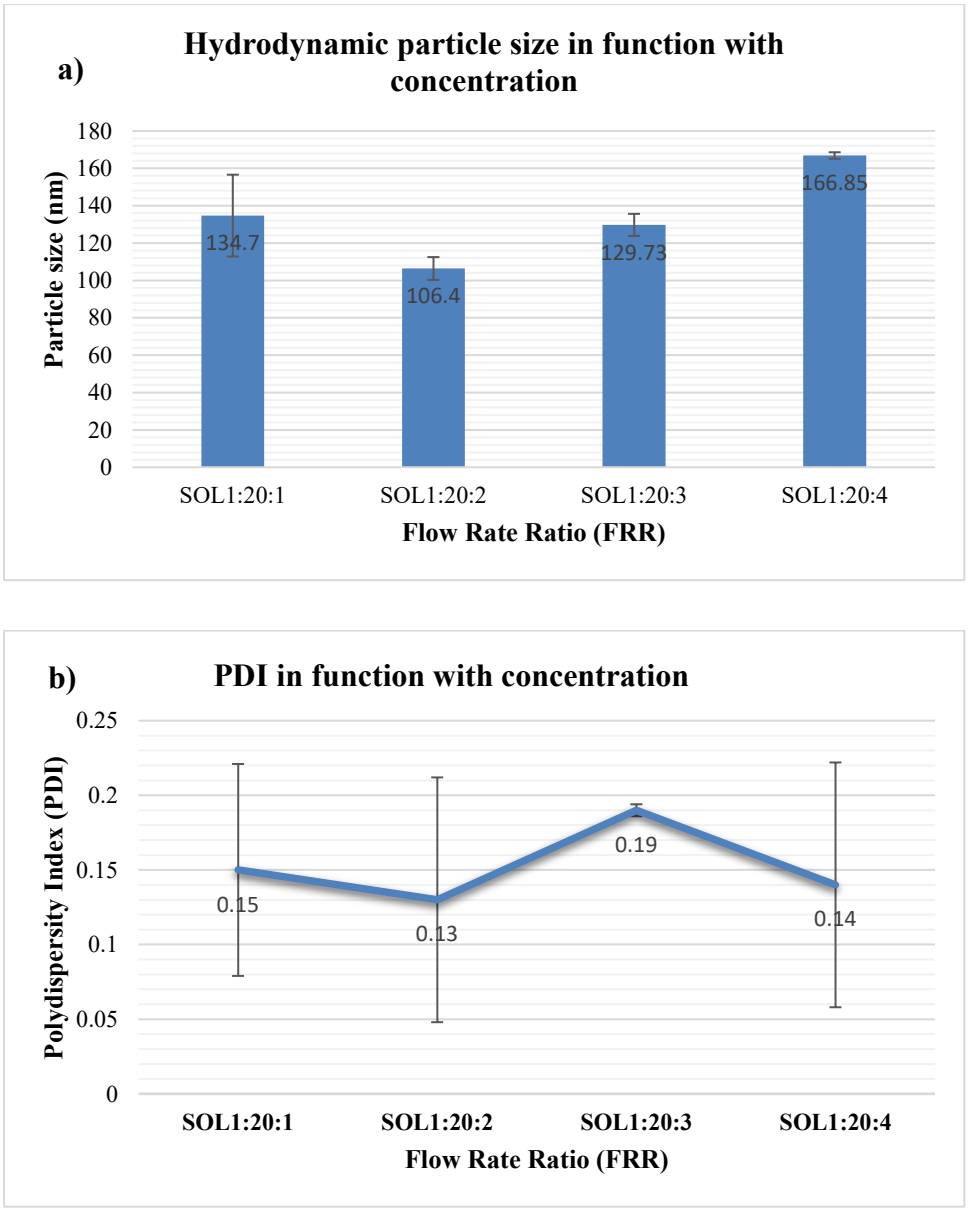

Figure 3.7 a) Average hydrodynamic nanoparticle size measured in function with four different flow rate ratio (FRR) and b) corresponding PDI in response of different FRR were measure with Zetasizer Nano ZS. Standard deviation is presented for each value.

The hydrodynamic size of particle obtained at FRR SOL1:20:1 was 134.7±21.89 and PDI 0.15±0.07 nm and particle hydrodynamic size decreased to 106.4±6.1 nm and PDI 0.13±0.08 at FRR SOL1:20:2, from this point particles hydrodynamic size start to increase with increasing FRR . At the FRR SOL1:20:3, hydrodynamic size of particles was 129.73±5.91 nm, PDI 0.19±0.003 and zeta potential -15.5 mV. The hydrodynamic

size of particles reached to 166.85±1.76 at FRR SOL1:20:4 while PDI value decreased to 0.14±0.08.

3.2.2 Morphological analysis of hybrid nanoparticles by TEM

Nanoprecipitate obtained from FRR of SOL1:20:1, SOL1:20:2, SOL1:20:3 and SOL1:20:4 ml/hr were used for the TEM image analysis. Precipitate was dispersed with acetone and carbon-coated grid were prepared for TEM image analysis. The results obtained by TEM concluded that the FRR SOL1:20:3 ml/hr has nanoparticles and at other flow rate no particles were observed. Whereas, few nanoparticles were spotted at the FRR of SOL1:20:4 ml/hr. The TEM image of FRR SOL1:20:3 is presented in figure 3.8.

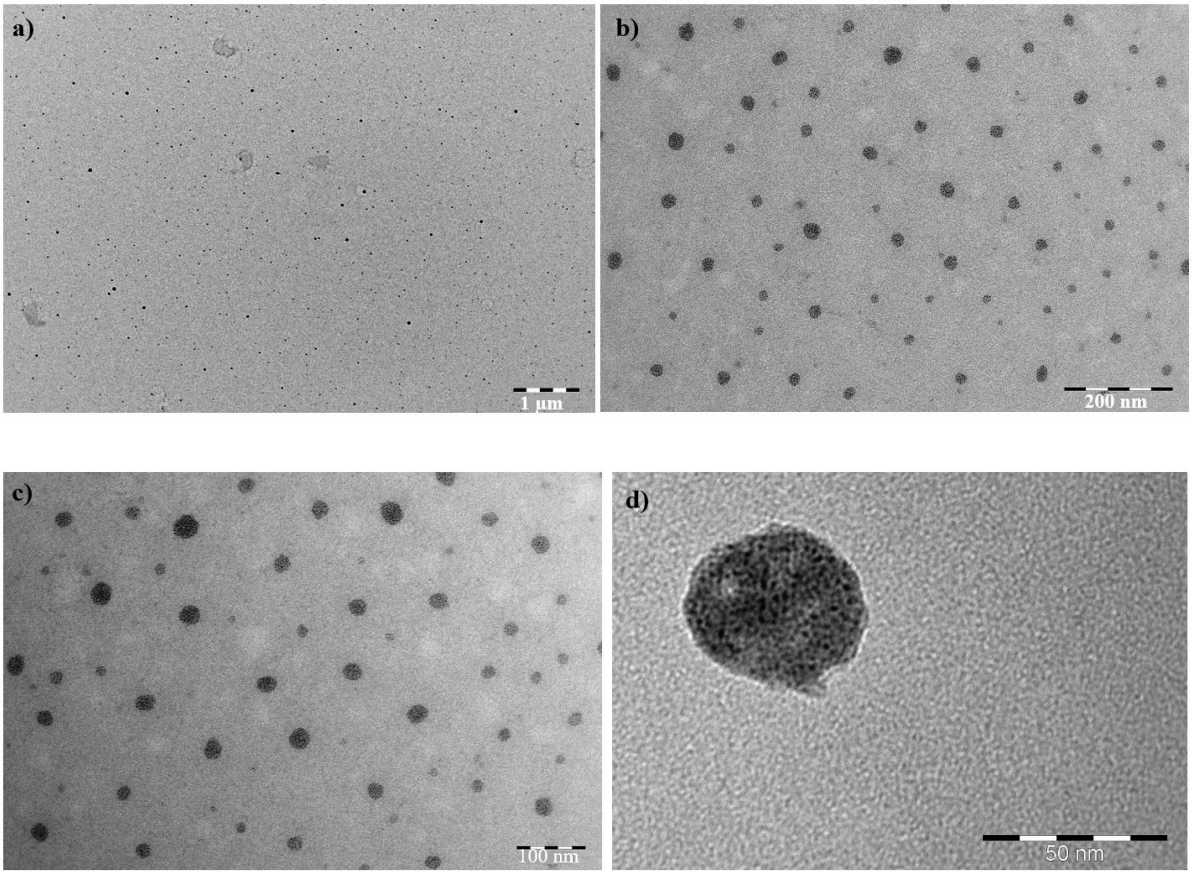

Figure 3.8 TEM image of lignin nanoparticles with size ranging from 20 to 50 nm a) low magnification at 8000X TEM image of lignin nanoparticles, scale bar: 1 µm, b) lignin nanoparticles image with magnification of 25,000X, scale bar: 200 nm, c) image of nanoparticles with scale bar of 100 nm and d) image of lignin nanoparticles taken at 200,000X magnification, scale bar: 50 nm.

TEM image were taken at different magnification ranging from 8,000X to 200,000X. The size of particles ranged from 20 to 50 nm in diameter. Morphological analysis by TEM indicates that the synthesized nanoparticles were of hybrid nature. Ultra-small primary nanoparticles between 2 to 4 nm were found trapped the matrix of different material that aided to glue primary particles together to form spherical nanoparticles of size range from 20 to 50 nm.

For the conformation, TEM image of solution obtained from two tapered end chip and the solution obtained from one tapered end chip were taken (figure 3.9).

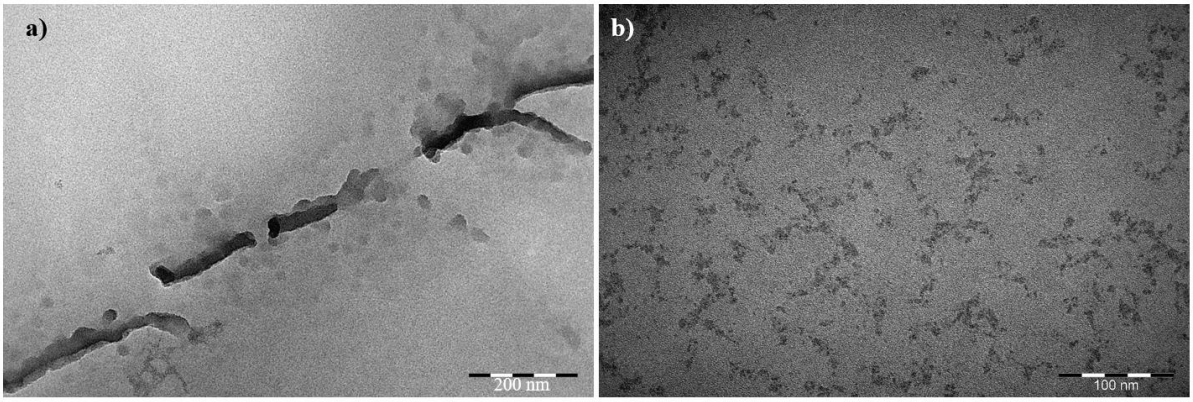

Figure 3.9 a) TEM image of lignin nanoprecipitate derived from two tapered end microfluidic chip with optimum flow rate set by the experiment (2:20:1 ml/hr), scale bar: 200 nm and b) TEM image of lignin nanoprecipitate obtain by one tapered end microfluidic chip with FRR of 2:20:3 ml/hr, scale bar:100 nm.

Analysis of TEM image presented in figure 3.9 suggests, image (a) obtain from nanoprecipitate of two tapered end microfluidic chip with the FRR of 2:20:1 ml/hr, hybrid particles were not observed instead deposition of large non porous particles was seen that appeared to be the material giving rise to matrix structure. Contrarily, from one tapered end microfluidic chip with the flow rate of 2:20:3 ml/hr (2 is lignin, 20 is acetone and 3 is NaOH). We were able to observe ultra-small nanoparticles in coherence with morphology of primary nanoparticles observed in hybrid nanoparticles. When we plot the size distribution by number curve of particles obtained at FRR of SOL1:20:3, 2:20:1 (two tapered end chip) and 2:20:3 (one tapered end chip). We clearly see the tree

different peak of different flow rate (figure 3.10), where the peak of hybrid nanoparticles formation falls between the peak of two tapered end and one tapered end chip.

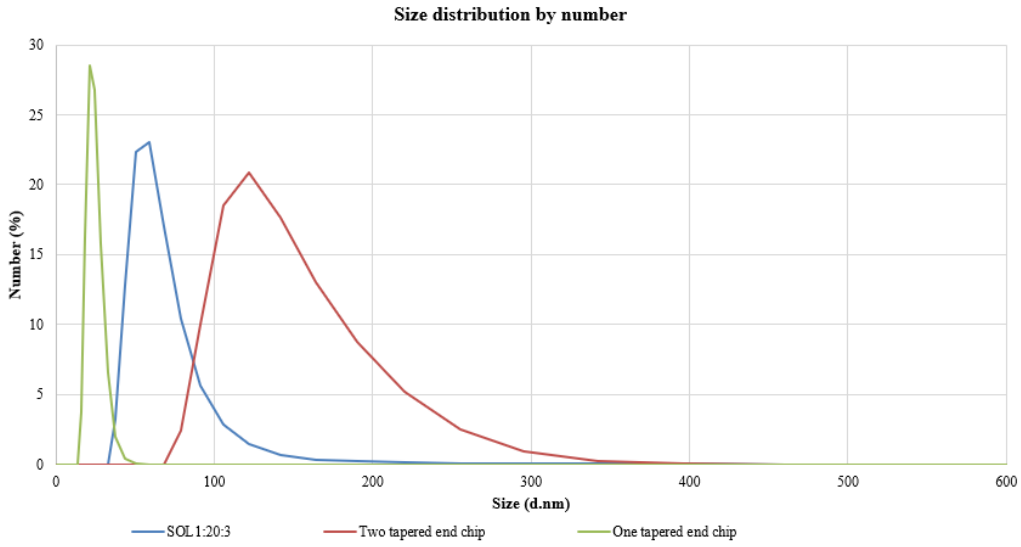

Figure 3.10 Representation of size distribution by number curve of optimized flow rate for hybrid nanoparticles, two tapered end and one tapered end microfluidic chip.

Therefore, based on TEM image and size distribution by number curve presented above, it can be concluded that the fabrication of hybrid nanoparticles from set of two microfluidics chip is the results of sequential precipitation. First matrix component is precipitated by the two tapered end microfluidics chip and then one tapered end microfluidic chip aids in assembly of matrix material into a nanocomposite and subsequently precipitates primary particles. Therefore, hybrid particles are fabricated when two processes i.e. matrix assembly into a nanoparticle and precipitation of primary nanoparticles are materialized simultaneously, as shown in figure 3.8. Synthesis of unique hybrid particles was achieved with the FRR of SOL1:20:3 ml/hr after successive series of optimization steps.

4. Discussion

The main objective of this project is to develop a method to fabricate lignin nanoparticles applying microfluidics platform. The kraft lignin (UPM BioPiva^{TM} 395) was used for this project. Lignin was selected because of unique properties such as resistance to decaying, UV absorbance, high stiffness and antioxidants. These properties make lignin suitable material for producing high value products (Beisl, Miltner, et al., 2017). Lignin is a polymer composed of three monomer units of p-coumaryl, coniferyl and sinapyl alcohol (Kun & Pukánszky, 2017). These monomers are covalently interconnected with primary linkage of C-C (condensed bonds) and C-O-C (ether bonds) to form a polymers (Henriksson, 2017). Chemical structure of lignin is highly branched with various functional group such as methoxy, carboxylic, phenolic and aliphatic hydroxyl, and carbonyl (Adler, 1977), these group can be modify to produce new material.

In this study microfluidics technology was used for synthesizing nanoparticles. Nanoprecipitation is one of the most widely used techniques for the production of the nanoparticles (Martínez Rivas et al., 2017). Here we apply microfluidics techniques for the fabrication of nanoparticles because it requires comparatively small reagents, short response time, low cost and the chances of contamination is very low (Igata et al., 2002).

4.1 Optimization lignin nanoparticle synthesis

Microfluidics devices are composed of millimeter scale fluidics channels which allow high surface to volume ratio and requires small volume of reagents (Paik et al., 2008). There are several bulk methods for the fabrication of nanoparticles, but the colloidal dispersions of nanoparticles fabricated by bulk method have several challenges to obtain uniform size distribution and reproducibility of semiconductor quantum dots (QD) (Jahn et al., 2008).

To fabricate lignin nanoparticles with microfluidics, flow rate ratio (FRR) between outer and inner fluids was optimized by performing several experiments (section 3.1 and 3.2). It is well known that flow rate impacts the physiochemical properties such as

hydrodynamic size and size distribution of nanoparticles (Abstiens & Goepferich, 2019). Based on the experiments, FRR 2:20:1 ml/hr was selected as the optimum flow rate of two tapered end microfluidics chip for nanoprecipitation. The selected flow rate was based on hydrodynamic flow focusing (HFF) technique (figure 1.3) where higher flow rate is employ to compress central solution with the lower flow rate from all direction, resulting in decreased diffusion distance and mixing time and eventually improve the quality of synthesized nanoparticles (Liu, Zhang, Fontana, et al., 2017). The hydrodynamic size and surface charge of particles was measured by dynamic light scattering (DLS). DLS gives a primary idea about the size of nanoparticles but does not measure the original size of the synthesized nanoparticles, the principle of DLS is describe in section 2.4.1.1.

During optimization, we were able to synthesize colloidal dispersion of monodispersed nanoparticles based on size PDI and zeta potential at the FRR 2:20:1 ml/hr. The theory of nucleation can help to explain the mechanism of it (Lamer & Dinegar, 1950). According to nucleation theory, ideally a system can promote seeding in a supersaturated concentration for a short time that followed by depletion of solute molecules for initiating particles growth by rapid diffusion, resulting nanoparticles are of uniform size distribution and low PDI (Jahn et al., 2008).

Zeta potential represents the stability of nanoparticles and measure repulsive force that help to keep particles separately and prevent aggregation. Zeta potential of selected optimized FRR is -24.6±2.17 mV, which is a net surface charge of the particles. According to Bhattacharjee, zeta potential in range of ±20-30 represent the particles are moderately stable colloidal dispersed. The PDI value represents uniform size distribution, PDI value ≤ 0.1 particles are highly monodispersed and value above 0.2 represents polydispersity of particles (Bhattacharjee, 2016). Colloidal dispersions of nanoparticles fabricated at FRR 2:20:1 ml/hr had hydrodynamic particle size of 162.5±1.82 nm, low PDI (0.12±0.017) and negative surface charge (-24.6±2.17 mV) indicates stable and monodispersed colloidal dispersion. Hence, the selected FRR (2:20:1 ml/hr) had optimum parameters for fabricating nanoparticles.

4.2 Morphology of lignin nanoparticles

Morphological analysis of nanoparticles is done with the transmission electron microscopy (TEM). TEM images showed porous lignin nanoparticles as shown in the image presented in figure 3.4 and 3.5. To confirm the results, we repeated our experiment several times, unfortunately results were not reproducible. However, in some experiment we observed the porous nanoparticles in smaller quantities in few sections of grid. Such type of porous nanoparticles was not reported from the lignin. Based on literature, reported lignin nanoparticles are spherical nanoparticles, nanotubes, nanofibers and hydrogels (Figueiredo et al., 2018). Therefore, we interested to fabricate such porous nanoparticles. With the suggestion of supervisors, we try to elucidate the reason behind obtaining few porous nanoparticles in some of the experiment. Lignin used for this project was impure and the chemical characterization is unknown thus we do not have any evidence to characterize the porous particles. Finally, we come up with two hypothesis, first one is that the porous nanoparticles might be present in the lignin but it may present in small quantities so it cannot be precipitated with the present setup of microfluidics chip and the second on is that these nanoparticles might be the hybrid particles and it way require sequential precipitation.

Schematic representation of microfluidics chip design for the sequential precipitation is represented in the figure 2.2. and the optimization of flow rate is described in section 3.2.1. Based on the hydrodynamic size and PDI value of particles, we select FRR SOL1:20:1, SOL1:20:2: SOL1:20:3 and SOL1:20:4 for TEM image analysis. TEM results manifest porous type nanoparticles at the FRR of SOL1:20:3 and comparatively few nanoparticles at FRR SOL1:20:4. However, we did not obtain any particles at lower flow rate concentration of NaOH i.e. at FRR of SOL1:20:1 and SOL1:20:2 and the number of particles also decreased with the increasing concentration of NaOH. These results suggest that the flow rate of NaOH (0.1 M) play important role for the nanoprecipitation by ionizing acid presented in lignin. It also support the antisolvent nanoprecipitation method, which suggest the raw lignin should be soluble in selected solvent based on the type of lignin and their extraction process (Lievonen et al., 2016).

4.2.1 Morphology of hybrid particles

TEM image obtains from the sequential precipitation is presented in figure 3.8, the morphological analysis of nanoparticles shows the nanoparticles are of hybrid nature. TEM images were taken on various magnification and the magnified image indicate the nanoparticles are made of two material. When we analysed the magnified image of TEM, it can be suggested that synthesized nanoparticle is the combination of ultra-small (2-4 nm) nanoparticles is trapped in the matrix of another material aided to glue primary nanoparticles together to form spherical nanoparticles of range 20 to 50 nm in diameter (figure 3.8. d). Such type of lignin-based nanoparticles was not reported yet. Several types of lignin-based nanoparticles were reported such as spherical, non-spherical, colloidal spherical, nano capsules, nanotubes and nanofibers (Figueiredo et al., 2018; Gao & Fatehi, 2019b). Lignin is utilized to fabricate organic-inorganic hybrid nanoparticles such as mesoporous lignin/silica hybrid nanoparticles by sol-gel method (Qu et al., 2010). Microfluidic nanoprecipitation approach effectively used in capsulate inorganic nanoparticles such as porous silicon, iron oxide gold nanoparticles within organic nanomatrix to produce hybrid nanoparticles for biomedical application (Y. Kim et al., 2013; Liu, Zhang, Cito, et al., 2017). Lignin structure consists of sufficient amount of different oxygen containing group that allow physical adsorption, hydrogen bonding, coordination, covalent linkage and acid-base interaction with other compounds (Telysheva et al., 2009). Whereas, presence of hydroxyl groups in lignin structure can help to incorporate lignin into silica structure to modify its pores, leading lignin/silica hybrid particle (Qu et al., 2010). Recently, lignin/silica hybrid nanoparticles functionalized with sulfonic acid-terminated polyamidoamine was synthesized by sol-gel method (Ahmadi & Abdollahi, 2020). Lignin composition varies from species to species and it also varies with the extraction process. Lignin consists of different functional groups i.e. aliphatic and aromatic hydroxyl, carbolic acid and ether linkage (Kumar, Kumar, & Bhowmik, 2018). Three stage mixing microfluidic device were used to prepare hollow structure lipid-polymer hybrid nanoparticles to entrap hydrophilic therapeutics like small interfering RNA (L. Zhang et al., 2015). Since, we used microfluidics device for sequential precipitation so it is possible to entrap some molecules within matrix as lignin used for this project is impure and it might consist of

different materials. Therefore, hybrid lignin nanoparticles fabricated by microfluidics assisted sequential nanoprecipitation need more detail chemical and morphological characterization which shall be undertaken as a future endeavor.

To investigate mechanism of hybrid lignin nanoparticles synthesis, product obtained from double tapered end chip and single tapered end chip, was analyzed with TEM microscopy. Results showed that double tapered end chip produced large non-porous particles or polymer aggregates whereas, ultra-small nanoparticles were obtained from single tapered end chip that resembled the primary nanoparticles observed in hybrid lignin nanoparticles. However, fabrication of hybrid lignin nanoparticles was only possible when lignin was processed in a sequential manner, first by double tapered end chip, followed by single tapered end chip. Hence it is concluded that hybrid lignin nanoparticles are fabricated through sequential precipitation. First matrix component is precipitated as polymer particles or aggregates, in the presence of acetone and NaOH in the double tapered end chip whereas primary particles were precipitated in the single tapered end chip. Subsequent self-assembly of matrix component of lignin around primary particles, results in enveloping of primary particles in the matrix component to fabricate hybrid lignin nanoparticles.

5. Conclusion

Microfluidics is an interdisciplinary subject to study microtechnology, engineering, biotechnology, chemistry, physics, and materials science. Here in this study, we develop and optimized microfluidics platform for the fabrication of hybrid nanoparticles from lignin. For the fabrication of nanoparticle, we design and prepare 3D hydrodynamic flow focusing devices (microfluidic chip) in our lab. Two type of microfluidics chip was utilized a) microfluidics chip with two tapered end and b) microfluidics chip with one tapered end. The optimum FRR for the two tapered end chip was 2:20:1 ml/hr (2 is 0.1% lignin, 20 is acetone and 1 is 0.1M NaOH) to optimally fabricate nanoparticle, the resulting nanoparticles average hydrodynamic size of 162.5±1.82 nm, PDI 0.12±0.017 and zeta potential -24.6±2.17 mV.

For the fabrication of hybrid nanoparticles, we used sequential precipitation method where we combine both microfluidics chip to develop optimum FRR for lignin nanoprecipitation. The optimum flow rate for the sequential precipitation was SOL1:20:3 ml/hr, where SOL1 is solution directly transferred at the rate of 23 ml/hr from two tapered end chip outlet to inner inlet of one tapered end chip, 20 (ml/hr) represents the flow rate of acetone and 1(ml/hr) represents flow rate of NaOH (0.1M) in the one tapered end chip outer inlet . The resulting average nanoparticles hydrodynamic size of 129.73±5.91 nm, PDI was 0.19±0.003 and zeta potential -15.5 mV.

TEM image analysis conclude that we were able to develop method to fabricate hybrid lignin nanoparticle of average size 20-50 nm by sequential precipitation method with optimum FRR of SOL1:20:3 by using microfluidics platform. Hybrid nanoparticles can be used for multiple function such as to deliver multi-drug to enhanced different diseases (cancer) treatment efficacy. Ones we characterized the hybrid nanoparticles then its application can be specified based on its biocompatibility.

6. Future perspective

Based on the investigation present in this study, interesting features and importance of lignin have been brought to light. Synthesized nanoparticle in this study is of unique and different structure then other lignin-based nanoparticles. Therefore, detail morphological analysis of this nanoparticles has to be done. Further study such as chemical characterization of the particles will help to understand the chemical constituent of nanoparticles. TEM image of present study suggest the nanoparticle is of hybrid nature or may consist of pore. For the characterization of chemical constituent of hybrid nanoparticle, it is important to characterize the ultra-small nanoparticle and matrix of hybrid nanoparticles. The characterization of hybrid material will open wide range of further study such as its biocompatibility with different cell line, utilizing as drug delivery for various diseases or using for different application.

7. References

Abstiens, K., & Goepferich, A. M. (2019). Microfluidic manufacturing improves polydispersity of multicomponent polymeric nanoparticles. *Journal of Drug Delivery Science and Technology*, *49*, 433–439. https://doi.org/10.1016/j.jddst.2018.12.009

Adler, E. (1977). Lignin chemistry-past, present and future. *Wood Science and Technology*, *11*(3), 169–218. https://doi.org/10.1007/BF00365615

Ahmadi, H., & Abdollahi, M. (2020). Synthesis and structural characterization of lignin/silica hybrid nanoparticles functionalized with sulfonic acid-terminated polyamidoamine. *Wood Science and Technology*, *54*(1), 249–268. https://doi.org/10.1007/s00226-019-01153-5

Alexandre, M., & Dubois, P. (2000). Polymer-layered silicate nanocomposites: Preparation, properties and uses of a new class of materials. *Materials Science and Engineering R: Reports*, *28*(1), 1–63. https://doi.org/10.1016/S0927-796X(00)00012-7

Beisl, S., Friedl, A., & Miltner, A. (2017, November 8). Lignin from micro- To nanosize: Applications. *International Journal of Molecular Sciences*, Vol. 18, p. 2367. https://doi.org/10.3390/ijms18112367

Beisl, S., Miltner, A., & Friedl, A. (2017, June 10). Lignin from micro- to nanosize: Production methods. *International Journal of Molecular Sciences*, Vol. 18. https://doi.org/10.3390/ijms18061244

Belgacem, M. N., Blayo, A., & Gandini, A. (2003). Organosolv lignin as a filler in inks, varnishes and paints. *Industrial Crops and Products*, *18*(2), 145–153. https://doi.org/10.1016/S0926-6690(03)00042-6

Bhattacharjee, S. (2016, August 10). DLS and zeta potential - What they are and what they are not? *Journal of Controlled Release*, Vol. 235, pp. 337–351. https://doi.org/10.1016/j.jconrel.2016.06.017

Bhaviripudi, S., Mile, E., Steiner, S. A., Zare, A. T., Dresselhaus, M. S., Belcher, A. M., & Kong, J. (2007). CVD synthesis of single-walled carbon nanotubes from gold nanoparticle catalysts. *Journal of the American Chemical Society*, *129*(6), 1516–1517. https://doi.org/10.1021/ja0673332

Boken, J., Soni, S. K., & Kumar, D. (2016). Microfluidic Synthesis of Nanoparticles and their Biosensing Applications. *Critical Reviews in Analytical Chemistry*, *46*(6),

538–561. https://doi.org/10.1080/10408347.2016.1169912

Burger, R., & Ducrée, J. (2012, May). Handling and analysis of cells and bioparticles on centrifugal microfluidic platforms. *Expert Review of Molecular Diagnostics*, Vol. 12, pp. 407–421. https://doi.org/10.1586/erm.12.28

Chen, H. (2015). Lignocellulose biorefinery feedstock engineering. In *Lignocellulose Biorefinery Engineering* (pp. 37–86). https://doi.org/10.1016/b978-0-08-100135-6.00003-x

de Gonzalo, G., Colpa, D. I., Habib, M. H. M., & Fraaije, M. W. (2016, October 20). Bacterial enzymes involved in lignin degradation. *Journal of Biotechnology*, Vol. 236, pp. 110–119. https://doi.org/10.1016/j.jbiotec.2016.08.011

Dunne, P. W., Munn, A. S., Starkey, C. L., Huddle, T. A., & Lester, E. H. (2015, December 28). Continuous-flow hydrothermal synthesis for the production of inorganic nanomaterials. *Philosophical Transactions of the Royal Society A: Mathematical, Physical and Engineering Sciences*, Vol. 373. https://doi.org/10.1098/rsta.2015.0015

Ealias, A. M., & Saravanakumar, M. P. (2017). A review on the classification, characterisation, synthesis of nanoparticles and their application. *IOP Conference Series: Materials Science and Engineering*, *263*(3), 032019. https://doi.org/10.1088/1757-899X/263/3/032019

Egerton, R. F. (2016). Physical principles of electron microscopy: An introduction to TEM, SEM, and AEM, second edition. In *Physical Principles of Electron Microscopy: An Introduction to TEM, SEM, and AEM, Second Edition*. https://doi.org/10.1007/978-3-319-39877-8

Egerton, Ray F. (2005). Physical principles of electron microscopy: An introduction to TEM, SEM, and AEM. In *Physical Principles of Electron Microscopy: An Introduction to TEM, SEM, and AEM*. https://doi.org/10.1007/b136495

Fernandes, E. M., Pires, R. A., Mano, J. F., & Reis, R. L. (2013, October 1). Bionanocomposites from lignocellulosic resources: Properties, applications and future trends for their use in the biomedical field. *Progress in Polymer Science*, Vol. 38, pp. 1415–1441. https://doi.org/10.1016/j.progpolymsci.2013.05.013

Figueiredo, P., Lintinen, K., Hirvonen, J. T., Kostiainen, M. A., & Santos, H. A. (2018, April 1). Properties and chemical modifications of lignin: Towards lignin-based

nanomaterials for biomedical applications. *Progress in Materials Science*, Vol. 93, pp. 233–269. https://doi.org/10.1016/j.pmatsci.2017.12.001

Frangville, C., Rutkevičius, M., Richter, A. P., Velev, O. D., Stoyanov, S. D., & Paunov, V. N. (2012). Fabrication of environmentally biodegradable lignin nanoparticles. *ChemPhysChem*, *13*(18), 4235–4243. https://doi.org/10.1002/cphc.201200537

Furth, M. E., Atala, A., & Van Dyke, M. E. (2007). Smart biomaterials design for tissue engineering and regenerative medicine. *Biomaterials*, *28*(34), 5068–5073. https://doi.org/10.1016/j.biomaterials.2007.07.042

Ganesh Kumar, C., Poornachandra, Y., & Pombala, S. (2017). Therapeutic nanomaterials: from a drug delivery perspective. In *Nanostructures for Drug Delivery* (pp. 1–61). https://doi.org/10.1016/b978-0-323-46143-6.00001-4

Gao, W., & Fatehi, P. (2019a). Lignin for polymer and nanoparticle production: Current status and challenges. *The Canadian Journal of Chemical Engineering*, *97*(11), 2827–2842. https://doi.org/10.1002/cjce.23620

Gao, W., & Fatehi, P. (2019b). Lignin for polymer and nanoparticle production: Current status and challenges. *The Canadian Journal of Chemical Engineering*, *97*(11), 2827–2842. https://doi.org/10.1002/cjce.23620

Gupta, A. K., Mohanty, S., & Nayak, S. K. (2015). Influence of addition of vapor grown carbon fibers on mechanical, thermal and biodegradation properties of lignin nanoparticle filled bio-poly(trimethylene terephthalate) hybrid nanocomposites. *RSC Advances*, *5*(69), 56028–56036. https://doi.org/10.1039/c5ra07828h

Hendriks, A. T. W. M., & Zeeman, G. (2009, January 1). Pretreatments to enhance the digestibility of lignocellulosic biomass. *Bioresource Technology*, Vol. 100, pp. 10–18. https://doi.org/10.1016/j.biortech.2008.05.027

Henriksson, G. (2017). What are the biological functions of lignin and its complexation with carbohydrates? *Nordic Pulp and Paper Research Journal*, *32*(4), 527–541. https://doi.org/10.3183/NPPRJ-2017-32-04-p527-541

Holladay, J. E., Bozell, J. J., White, J. F., & Johnson, D. (2007). *Top Value-Added Chemicals from Biomass - Volume II—Results of Screening for Potential Candidates from Biorefinery Lignin*. Retrieved from http://www.ntis.gov/ordering.htm

Hu, S., & Hsieh, Y. Lo. (2016). Silver nanoparticle synthesis using lignin as reducing and capping agents: A kinetic and mechanistic study. *International Journal of Biological Macromolecules*, *82*, 856–862.

https://doi.org/10.1016/j.ijbiomac.2015.09.066

Igata, E., Arundell, M., Morgan, H., & Cooper, J. M. (2002). Interconnected reversible lab-on-a-chip technology. *Lab on a Chip*, *2*(2), 65–69. https://doi.org/10.1039/b200928p

Itoh, H., Wada, M., Honda, Y., Kuwahara, M., & Watanabe, T. (2003). Bioorganosolve pretreatments for simultaneous saccharification and fermentation of beech wood by ethanolysis and white rot fungi. *Journal of Biotechnology*, *103*(3), 273–280. https://doi.org/10.1016/S0168-1656(03)00123-8

Jahn, A., Reiner, J. E., Vreeland, W. N., DeVoe, D. L., Locascio, L. E., & Gaitan, M. (2008, August 15). Preparation of nanoparticles by continuous-flow microfluidics. *Journal of Nanoparticle Research*, Vol. 10, pp. 925–934. https://doi.org/10.1007/s11051-007-9340-5

Janasek, D., Franzke, J., & Manz, A. (2006, July 27). Scaling and the design of miniaturized chemical-analysis systems. *Nature*, Vol. 442, pp. 374–380. https://doi.org/10.1038/nature05059

Janczak, C. M., & Aspinwall, C. A. (2012). Composite nanoparticles: The best of two worlds. *Analytical and Bioanalytical Chemistry*, *402*(1), 83–89. https://doi.org/10.1007/s00216-011-5482-5

Johnson, B. K., & Prud'homme, R. K. (2003). Mechanism for rapid self-assembly of block copolymer nanoparticles. *Physical Review Letters*, *91*(11), 118302. https://doi.org/10.1103/PhysRevLett.91.118302

Kai, D., Tan, M. J., Chee, P. L., Chua, Y. K., Yap, Y. L., & Loh, X. J. (2016, February 29). Towards lignin-based functional materials in a sustainable world. *Green Chemistry*, Vol. 18, pp. 1175–1200. https://doi.org/10.1039/c5gc02616d

Kai, D., Zhang, K., Jiang, L., Wong, H. Z., Li, Z., Zhang, Z., & Loh, X. J. (2017). Sustainable and Antioxidant Lignin-Polyester Copolymers and Nanofibers for Potential Healthcare Applications. *ACS Sustainable Chemistry and Engineering*, *5*(7), 6016–6025. https://doi.org/10.1021/acssuschemeng.7b00850

Kammler, H. K., Mädler, L., & Pratsinis, S. E. (2001). Flame synthesis of nanoparticles. *Chemical Engineering and Technology*, *24*(6), 583–596. https://doi.org/10.1002/1521-4125(200106)24:6<583::AID-CEAT583>3.0.CO;2-H

Kim, B. Y. S., Rutka, J. T., & Chan, W. C. W. (2010, December 16). Current concepts: Nanomedicine. *New England Journal of Medicine*, Vol. 363, pp. 2434–2443. https://doi.org/10.1056/NEJMra0912273

Kim, Y., Fay, F., Cormode, D. P., Sanchez-Gaytan, B. L., Tang, J., Hennessy, E. J., … Fayad, Z. A. (2013). Single step reconstitution of multifunctional high-density lipoprotein-derived nanomaterials using microfluidics. *ACS Nano*, *7*(11), 9975–9983. https://doi.org/10.1021/nn4039063

Konnerth, H., Zhang, J., Ma, D., Prechtl, M. H. G., & Yan, N. (2015). Base promoted hydrogenolysis of lignin model compounds and organosolv lignin over metal catalysts in water. *Chemical Engineering Science*, *123*, 155–163. https://doi.org/10.1016/j.ces.2014.10.045

Kumar, R., Kumar, K., & Bhowmik, S. (2018). Mechanical characterization and quantification of tensile, fracture and viscoelastic characteristics of wood filler reinforced epoxy composite. *Wood Science and Technology*, *52*(3), 677–699. https://doi.org/10.1007/s00226-018-0995-0

Kun, D., & Pukánszky, B. (2017, August 1). Polymer/lignin blends: Interactions, properties, applications. *European Polymer Journal*, Vol. 93, pp. 618–641. https://doi.org/10.1016/j.eurpolymj.2017.04.035

Lamer, V. K., & Dinegar, R. H. (1950). Theory, Production and Mechanism of Formation of Monodispersed Hydrosols. *Journal of the American Chemical Society*, *72*(11), 4847–4854. https://doi.org/10.1021/ja01167a001

Laurichesse, S., & Avérous, L. (2014, July 1). Chemical modification of lignins: Towards biobased polymers. *Progress in Polymer Science*, Vol. 39, pp. 1266–1290. https://doi.org/10.1016/j.progpolymsci.2013.11.004

Lepeltier, E., Bourgaux, C., & Couvreur, P. (2014, May 1). Nanoprecipitation and the "Ouzo effect": Application to drug delivery devices. *Advanced Drug Delivery Reviews*, Vol. 71, pp. 86–97. https://doi.org/10.1016/j.addr.2013.12.009

Li, W., Zhang, L., Ge, X., Xu, B., Zhang, W., Qu, L., … Weitz, D. A. (2018, August 7). Microfluidic fabrication of microparticles for biomedical applications. *Chemical Society Reviews*, Vol. 47, pp. 5646–5683. https://doi.org/10.1039/c7cs00263g

Li, X., Ballerini, D. R., & Shen, W. (2012, March 2). A perspective on paper-based microfluidics: Current status and future trends. *Biomicrofluidics*, Vol. 6, p. 011301. https://doi.org/10.1063/1.3687398

Lievonen, M., Valle-Delgado, J. J., Mattinen, M. L., Hult, E. L., Lintinen, K.,

Kostiainen, M. A., … Österberg, M. (2016). A simple process for lignin nanoparticle preparation. *Green Chemistry*, *18*(5), 1416–1422. https://doi.org/10.1039/c5gc01436k

Lin, N., Fan, D., Chang, P. R., Yu, J., Cheng, X., & Huang, J. (2011). Structure and properties of poly(butylene succinate) filled with lignin: A case of lignosulfonate. *Journal of Applied Polymer Science*, *121*(3), 1717–1724. https://doi.org/10.1002/app.33754

Liu, D., Zhang, H., Cito, S., Fan, J., Mä, E., Salonen, J., … Paulson, J. A. (2017). Core/Shell Nanocomposites Produced by Superfast Sequential Microfluidic Nanoprecipitation. *ACS Publications*, *17*(2), 606–614. https://doi.org/10.1021/acs.nanolett.6b03251

Liu, D., Zhang, H., Fontana, F., Hirvonen, J. T., & Santos, H. A. (2017, June 7). Microfluidic-assisted fabrication of carriers for controlled drug delivery. *Lab on a Chip*, Vol. 17, pp. 1856–1883. https://doi.org/10.1039/c7lc00242d

Lora, J. H., & Glasser, W. G. (2002). Recent industrial applications of lignin: A sustainable alternative to nonrenewable materials. *Journal of Polymers and the Environment*, *10*(1–2), 39–48. https://doi.org/10.1023/A:1021070006895

Lu, M., Ozcelik, A., Grigsby, C. L., Zhao, Y., Guo, F., Leong, K. W., & Huang, T. J. (2016, December 1). Microfluidic hydrodynamic focusing for synthesis of nanomaterials. *Nano Today*, Vol. 11, pp. 778–792. https://doi.org/10.1016/j.nantod.2016.10.006

Lu, Q., Zhu, M., Zu, Y., Liu, W., Yang, L., Zhang, Y., … Li, W. (2012). Comparative antioxidant activity of nanoscale lignin prepared by a supercritical antisolvent (SAS) process with non-nanoscale lignin. *Food Chemistry*, *135*(1), 63–67. https://doi.org/10.1016/j.foodchem.2012.04.070

Malhotra, B. D., & Ali, M. A. (2018). Microfluidic Biosensor. In *Nanomaterials for Biosensors* (pp. 263–293). https://doi.org/10.1016/b978-0-323-44923-6.00009-1

Martínez Rivas, C. J., Tarhini, M., Badri, W., Miladi, K., Greige-Gerges, H., Nazari, Q. A., … Elaissari, A. (2017, October 30). Nanoprecipitation process: From encapsulation to drug delivery. *International Journal of Pharmaceutics*, Vol. 532, pp. 66–81. https://doi.org/10.1016/j.ijpharm.2017.08.064

Minteer, S. (2006). *Microfluidic techniques: reviews and protocols*. Retrieved from

https://www.google.com/books?hl=en&lr=&id=Rqb6TbrihpcC&oi=fnd&pg=PA2&dq=S.D.+Minteer,+Microfluidic+Techniques:+Reviews+and+Protocols,+vol.+321,+Springer,+2006&ots=Iq5HyFPGhp&sig=AegWoDfCm0mHUs7K6EEOGJmQwB0

Mishra, P. K., & Wimmer, R. (2017). Aerosol assisted self-assembly as a route to synthesize solid and hollow spherical lignin colloids and its utilization in layer by layer deposition. *Ultrasonics Sonochemistry*, *35*, 45–50. https://doi.org/10.1016/j.ultsonch.2016.09.001

Missana, T., & Adell, A. (2000). On the applicability of DLVO theory to the prediction of clay colloids stability. *Journal of Colloid and Interface Science*, *230*(1), 150–156. https://doi.org/10.1006/jcis.2000.7003

Mohammadi, S., Harvey, A., & Boodhoo, K. V. K. (2014). Synthesis of TiO2 nanoparticles in a spinning disc reactor. *Chemical Engineering Journal*, *258*, 171–184. https://doi.org/10.1016/j.cej.2014.07.042

Mohapatra, S., Nguyen, T. A., & Nguyen-Tri, P. (2018). Noble metal-metal oxide hybrid nanoparticles: Fundamentals and applications. In *Noble Metal-Metal Oxide Hybrid Nanoparticles: Fundamentals and Applications*. https://doi.org/10.1016/C2017-0-00847-9

Nge, P. N., Rogers, C. I., & Woolley, A. T. (2013, April 10). Advances in microfluidic materials, functions, integration, and applications. *Chemical Reviews*, Vol. 113, pp. 2550–2583. https://doi.org/10.1021/cr300337x

Norgren, M., & Edlund, H. (2014, October 1). Lignin: Recent advances and emerging applications. *Current Opinion in Colloid and Interface Science*, Vol. 19, pp. 409–416. https://doi.org/10.1016/j.cocis.2014.08.004

Paik, P. Y., Pamula, V. K., & Chakrabarty, K. (2008). A digital-microfluidic approach to chip cooling. *IEEE Design and Test of Computers*, *25*(4), 372–391. https://doi.org/10.1109/MDT.2008.87

Pallandre, A., de Lambert, B., Attia, R., Jonas, A. M., & Viovy, J. L. (2006, February 1). Surface treatment and characterization: Perspectives to electrophoresis and lab-on-chips. *Electrophoresis*, Vol. 27, pp. 584–610. https://doi.org/10.1002/elps.200500761

Pandey, M. P., & Kim, C. S. (2011, January 1). Lignin Depolymerization and Conversion: A Review of Thermochemical Methods. *Chemical Engineering and Technology*, Vol. 34, pp. 29–41. https://doi.org/10.1002/ceat.201000270

Park, J. Il, Saffari, A., Kumar, S., Günther, A., & Kumacheva, E. (2010). Microfluidic Synthesis of Polymer and Inorganic Particulate Materials. *Annual Review of Materials Research*, *40*(1), 415–443. https://doi.org/10.1146/annurev-matsci-070909-104514

Pouteau, C., Dole, P., Cathala, B., Averous, L., & Boquillon, N. (2003). Antioxidant properties of lignin in polypropylene. *Polymer Degradation and Stability*, *81*(1), 9–18. https://doi.org/10.1016/S0141-3910(03)00057-0

Qian, Y., Deng, Y., Qiu, X., Li, H., & Yang, D. (2014). Formation of uniform colloidal spheres from lignin, a renewable resource recovered from pulping spent liquor. *Green Chemistry*, *16*(4), 2156–2163. https://doi.org/10.1039/c3gc42131g

Qu, Y., Tian, Y., Zou, B., Zhang, J., Zheng, Y., Wang, L., … Wang, Z. (2010). A novel mesoporous lignin/silica hybrid from rice husk produced by a sol-gel method. *Bioresource Technology*, *101*(21), 8402–8405. https://doi.org/10.1016/j.biortech.2010.05.067

Ragauskas, A. J., Beckham, G. T., Biddy, M. J., Chandra, R., Chen, F., Davis, M. F., … Wyman, C. E. (2014, May 16). Lignin valorization: Improving lignin processing in the biorefinery. *Science*, Vol. 344. https://doi.org/10.1126/science.1246843

Rodríguez, A., Sánchez, R., Requejo, A., & Ferrer, A. (2010). Feasibility of rice straw as a raw material for the production of soda cellulose pulp. *Journal of Cleaner Production*, *18*(10–11), 1084–1091. https://doi.org/10.1016/j.jclepro.2010.03.011

Samyn, P., Barhoum, A., Öhlund, T., & Dufresne, A. (2018). Review: nanoparticles and nanostructured materials in papermaking. *Journal of Materials Science*, *53*(1), 146–184. https://doi.org/10.1007/s10853-017-1525-4

Silverstein, R. A., Chen, Y., Sharma-Shivappa, R. R., Boyette, M. D., & Osborne, J. (2007). A comparison of chemical pretreatment methods for improving saccharification of cotton stalks. *Bioresource Technology*, *98*(16), 3000–3011. https://doi.org/10.1016/j.biortech.2006.10.022

Stetefeld, J., McKenna, S. A., & Patel, T. R. (2016, December 1). Dynamic light scattering: a practical guide and applications in biomedical sciences. *Biophysical Reviews*, Vol. 8, pp. 409–427. https://doi.org/10.1007/s12551-016-0218-6

Stone, H. A., Stroock, A. D., & Ajdari, A. (2004). ENGINEERING FLOWS IN SMALL DEVICES. *Annual Review of Fluid Mechanics*, *36*(1), 381–411.

https://doi.org/10.1146/annurev.fluid.36.050802.122124

Suhara, H., Kodama, S., Kamei, I., Maekawa, N., & Meguro, S. (2012). Screening of selective lignin-degrading basidiomycetes and biological pretreatment for enzymatic hydrolysis of bamboo culms. *International Biodeterioration and Biodegradation*, *75*, 176–180. https://doi.org/10.1016/j.ibiod.2012.05.042

Sun, Y., & Cheng, J. (2002). Hydrolysis of lignocellulosic materials for ethanol production: A review. *Bioresource Technology*, *83*(1), 1–11. https://doi.org/10.1016/S0960-8524(01)00212-7

Tai, C. Y., Tai, C. Te, Chang, M. H., & Liu, H. S. (2007). Synthesis of magnesium hydroxide and oxide nanoparticles using a spinning disk reactor. *Industrial and Engineering Chemistry Research*, *46*(17), 5536–5541. https://doi.org/10.1021/ie060869b

Tejado, A., Peña, C., Labidi, J., Echeverria, J. M., & Mondragon, I. (2007). Physico-chemical characterization of lignins from different sources for use in phenol-formaldehyde resin synthesis. *Bioresource Technology*, *98*(8), 1655–1663. https://doi.org/10.1016/j.biortech.2006.05.042

Telysheva, G., Dizhbite, T., Evtuguin, D., Mironova-Ulmane, N., Lebedeva, G., Andersone, A., … Belkova, L. (2009). Design of siliceous lignins - Novel organic/inorganic hybrid sorbent materials. *Scripta Materialia*, *60*(8), 687–690. https://doi.org/10.1016/j.scriptamat.2008.12.051

Ten, E., Ling, C., Wang, Y., Srivastava, A., Dempere, L. A., & Vermerris, W. (2014). Lignin nanotubes as vehicles for gene delivery into human cells. *Biomacromolecules*, *15*(1), 327–338. https://doi.org/10.1021/bm401555p

Terry, S. C., Herman, J. H., & Angell, J. B. (1979). A Gas Chromatographic Air Analyzer Fabricated on a Silicon Wafer. *IEEE Transactions on Electron Devices*, *26*(12), 1880–1886. https://doi.org/10.1109/T-ED.1979.19791

Tribot, A., Amer, G., Abdou Alio, M., de Baynast, H., Delattre, C., Pons, A., … Dussap, C. G. (2019, March 1). Wood-lignin: Supply, extraction processes and use as bio-based material. *European Polymer Journal*, Vol. 112, pp. 228–240. https://doi.org/10.1016/j.eurpolymj.2019.01.007

Tsaoulidis, D., & Angeli, P. (2015). Effect of channel size on mass transfer during liquid-liquid plug flow in small scale extractors. *Chemical Engineering Journal*, *262*, 785–793. https://doi.org/10.1016/j.cej.2014.10.012

Uson, L., Arruebo, M., Sebastian, V., & Santamaria, J. (2018). Single phase

microreactor for the continuous, high-temperature synthesis of amplt; 4 nm superparamagnetic iron oxide nanoparticles. https://doi.org/10.1016/j.cej.2017.12.024

Valášková, V., Šnajdr, J., Bittner, B., Cajthaml, T., Merhautová, V., Hofrichter, M., & Baldrian, P. (2007). Production of lignocellulose-degrading enzymes and degradation of leaf litter by saprotrophic basidiomycetes isolated from a Quercus petraea forest. *Soil Biology and Biochemistry*, *39*(10), 2651–2660. https://doi.org/10.1016/j.soilbio.2007.05.023

Van Den Berg, A., & Andersson, H. (2004). Microfabrication and microfluidics for tissue engineering: State of the art and future opportunities Sprintloc for the proteome View project Microfabrication and microfluidics for tissue engineering: state of the art and future opportunities. *Pubs.Rsc.Org*. https://doi.org/10.1039/b314469k

Vishtal, A., & Kraslawski, A. (2011, August). Challenges in industrial applications of technical lignins. *BioResources*, Vol. 6, pp. 3547–3568. https://doi.org/10.15376/biores.6.3.3547-3568

Xia, Y., Xiong, Y., Lim, B., & Skrabalak, S. E. (2009). Shape-Controlled Synthesis of Metal Nanocrystals : Simple. *Angewandte Chemie International Edition*, *48*(1), 60–103. https://doi.org/10.1002/anie.200802248.Shape-Controlled

Yearla, S. R., & Padmasree, K. (2016). Preparation and characterisation of lignin nanoparticles: evaluation of their potential as antioxidants and UV protectants. *Journal of Experimental Nanoscience*, *11*(4), 289–302. https://doi.org/10.1080/17458080.2015.1055842

Yeo, L. Y., Chang, H. C., Chan, P. P. Y., & Friend, J. R. (2011, January 3). Microfluidic devices for bioapplications. *Small*, Vol. 7, pp. 12–48. https://doi.org/10.1002/smll.201000946

Yiamsawas, D., Baier, G., Thines, E., Landfester, K., & Wurm, F. R. (2014). Biodegradable lignin nanocontainers. *RSC Advances*, *4*(23), 11661–11663. https://doi.org/10.1039/c3ra47971d

Zakzeski, J., Bruijnincx, P. C. A., Jongerius, A. L., & Weckhuysen, B. M. (2010). The catalytic valorization of lignin for the production of renewable chemicals. *Chemical Reviews*, *110*(6), 3552–3599. https://doi.org/10.1021/cr900354u

Zhang, J., Yan, S., Yuan, D., Alici, G., Nguyen, N. T., Ebrahimi Warkiani, M., & Li, W. (2016). Fundamentals and applications of inertial microfluidics: A review. *Lab on a Chip*, Vol. 16, pp. 10–34. https://doi.org/10.1039/c5lc01159k

Zhang, L., Feng, Q., Wang, J., Sun, J., Shi, X., & Jiang, X. (2015). Microfluidic Synthesis of Rigid Nanovesicles for Hydrophilic Reagents Delivery. *Angewandte Chemie*, *127*(13), 4024–4028. https://doi.org/10.1002/ange.201500096

Zhang, M., Gong, X., & Wen, W. (2009, September). Manipulation of microfluidic droplets by electrorheological fluid. *Electrophoresis*, Vol. 30, pp. 3116–3123. https://doi.org/10.1002/elps.200900119

Zhao, W., Simmons, B., Singh, S., Ragauskas, A., & Cheng, G. (2016). From lignin association to nano-/micro-particle preparation: Extracting higher value of lignin. *Green Chemistry*, Vol. 18, pp. 5693–5700. https://doi.org/10.1039/c6gc01813k

Zhao, X., Bian, F., Sun, L., Cai, L., Li, L., & Zhao, Y. (2020). Microfluidic Generation of Nanomaterials for Biomedical Applications. *Small*, *16*(9), 1901943. https://doi.org/10.1002/smll.201901943